remote sensing

MDPI

Article

Continental Shelf-Scale Passive Acoustic Detection and Characterization of Diesel-Electric Ships Using a Coherent Hydrophone Array

Wei Huang [1], Delin Wang [1], Heriberto Garcia [1], Olav Rune Godø [2] and Purnima Ratilal [1,*]

[1] Department of Electrical and Computer Engineering, Northeastern University, 360 Huntington Ave, Boston, MA 02115, USA; huang.wei1@husky.neu.edu (W.H.); wang.del@husky.neu.edu (D.W.); garcia.he@husky.neu.edu (H.G.)

[2] Institute of Marine Research, Post Office Box 1870, Nordnes, N-5817 Bergen, Norway; olav.rune.godoe@imr.no

* Correspondence: purnima@ece.neu.edu; Tel.: +1-617-373-8458

Received: 11 June 2017; Accepted: 24 July 2017; Published: 28 July 2017

Abstract: The passive ocean acoustic waveguide remote sensing (POAWRS) technique is employed to detect and characterize the underwater sound radiated from three scientific research and fishing vessels received at long ranges on a large-aperture densely-sampled horizontal coherent hydrophone array. The sounds radiated from the research vessel (RV) Delaware II in the Gulf of Maine, and the RV Johan Hjort and the fishing vessel (FV) Artus in the Norwegian Sea are found to be dominated by distinct narrowband tonals and cyclostationary signals in the 150 Hz to 2000 Hz frequency range. The source levels of these signals are estimated by correcting the received pressure levels for transmission losses modeled using a calibrated parabolic equation-based acoustic propagation model for random range-dependent ocean waveguides. The probability of the detection region for the most prominent signal radiated by each ship is estimated and shown to extend over areas spanning roughly 200 km in diameter when employing a coherent hydrophone array. The current standard procedure for quantifying ship-radiated sound source levels via one-third octave bandwidth intensity averaging smoothes over the prominent tonals radiated by a ship that can stand 10 to 30 dB above the local broadband level, which may lead to inaccurate or incorrect assessments of the impact of ship-radiated sound.

Keywords: ship noise; passive ocean acoustic waveguide remote sensing; source level; ship tonal

1. Introduction

The remote monitoring of ocean vehicles over instantaneous wide areas from their sounds radiated underwater is essential in maritime surveillance and defence [1–9]. The sound generated by ocean vehicles contributes to environmental ambient noise [10] which often limits detection ranges in passive and active sonar systems for a wide range of ocean remote sensing applications [1,9,11–14], as well as in ocean acoustic communication [15,16]. It may also impact the behavior and communication of marine organisms [17–20], such as fish [21–24] and marine mammals [25–27]. Ship-radiated sound may also impact fish stock abundance estimates based on conventional ultrasonic echosounding surveys due to potential avoidance reactions by fish populations to the approaching survey vessel [22–24,28–31].

Here we employ a large-aperture densely-sampled horizontal coherent hydrophone array consisting of 160 hydrophone elements, providing roughly two orders of magnitude higher array gain than a single hydrophone, to detect underwater sound radiated by surface ships over wide areas using the passive ocean acoustic waveguide remote sensing (POAWRS) technique. POAWRS was previously applied to detect, localize and classify the vocalization signals from multiple baleen

whale and toothed whale species [13,32–35] simultaneously over continental shelf-scale regions of approximately 100,000 km^2. Here the POAWRS approach is employed to detect and characterize the underwater sound radiated from three known surface ships which were received after long-range propagation on the coherent hydrophone array. The ships investigated here are the US research vessel (RV) Delaware II, as well as the Norwegian RV Johan Hjort and fishing vessel (FV) Artus, with accurately known locations obtained from global positioning systems (GPS) at ranges varying between 4 km to 32 km from the coherent hydrophone array.

Passive acoustic methods have been previously used to examine, characterize and quantify the sound radiated from surface ships, with most measurements in the published literature made using a single hydrophone [36,37] or a small number of widely-separated hydrophones [3,4,38] located from within a few hundred meters to a few kilometers away from a ship. Ship-radiated sound has also been measured using a 128-element vertical hydrophone array [39] and bottom-mounted hydrophones [40]. The mechanism of sound generation by ships is described in [9,28,41–46]. The main sources of ship radiated sound are: (1) machinery noise generated by propulsion and auxiliary machinery such as engines, main motors and gears; (2) propeller noise generated by cavitation at or near the propeller and propeller-induced resonant hull excitation; (3) hydrodynamic noise from radiated flow noise, resonant excitation of cavities, plates, and appendages; and (4) cavitation at struts and appendages. The passive acoustic spectra of ship-radiated sound is extremely dynamic, containing both broadband signals and narrowband tonals at discrete frequencies [23,41] with source levels that can vary depending on ship conditions [42,47] such as ship speed [48–50], orientation [39] and maneuvers [51]. Ship noise has been previously found to be dominated by propeller cavitation, propeller singing due to physical excitation at the trailing edges of the blades, and propulsion or other reciprocating machinery [2,8,18,28,45,46]. The nonlinear analysis of marine propeller noise is provided in [52,53].

We show that the underwater sounds radiated from the three surface ships investigated here and received at long ranges (4 km to 32 km) by the coherent hydrophone array are dominated by narrowband discrete tonals and cyclostationary signals. We estimate the source levels of the prominent tonals and cyclostationary signals radiated from each ship by correcting the received pressure levels for transmission losses modeled using a calibrated [54–57] parabolic equation-based acoustic propagation model [58,59] for random range-dependent ocean waveguides. The estimated source levels of the prominent ship-radiated tonals and cyclostationary signals are then applied to determine the probabilty of detection regions for each of the three surface ships, the RV Delaware II in the Gulf of Maine, and the RV Johan Hjort and the FV Artus in the Norwegian Sea. Here we show that by employing coherent beamforming of the horizontal hydrophone array data, the signals radiated by ships can be detected with high signal-to-noise ratios (SNR) leading to significantly enhanced detection regions compared to those of a single hydrophone.

The term 'signature' is commonly used to denote the levels [37] of underwater radiated noise versus frequency for an underwater vehicle spanning frequency ranges from roughly 10 Hz to 100 kHz. To enable comparison of ship-radiated sound across different ships, most ship noise ranging reports contain signatures in the form of averaged curves derived from measurements usually made in a one-third octave bandwidth, and then converted to a 1 Hz band [22,26–28]. Here we show that this 'signature' analysis smooths or averages out the dominant discrete tones radiated by a ship that are the key signals enabling ship detection at long ranges, and as a result can lead to significant underestimation of a ship's detection range and region or zone of acoustic interference or influence. This one-third octave bandwidth intensity averaging is also problematic for studies of the impact of ship noise on fish behavior. This is because the dominant narrowband tonal signals radiated from a ship that typically stand 10 dB to 30 dB above the local broadband levels are significantly reduced or disappear after one-third octave bandwidth intensity averaging. This tonal reduction or disappearance can become more severe with increasing frequency since the one-third octave bandwidths get progressively larger by a factor of $2^{1/3} = 1.26$ with increasing frequency. While the

overall one-third octave bandwidth intensity averaged ship sound source levels may be below the International Council for the Exploration of the Sea (ICES)-recommended Cooperative Research Report No. 209 (CRR 209, Mitson, 1995) levels , the individual tonal components can have levels that typically exceed the recommended levels by over 10 to 30 dB. The dominant high-level tonal signals radiated by a ship may be the primary sound field the fish and marine mammals are responding to, and must be included in studies of fish behavioral responses to ship-radiated sounds.

2. Materials and Methods

2.1. Measurement of Ship-Radiated Sound Using a Coherent Hydrophone Array

The underwater recordings of ship-radiated sound analyzed here are drawn from two separate experiments, the US Gulf of Maine 2006 Experiment (GOME06) where the RV Delaware II was present (Figure 1A), and the Norwegian Sea 2014 Experiment (NorEx14) where the FV Artus (Figure 1B) and the RV Johan Hjort (Figure 1C) were present. Both these experiments were conducted by a collaborative team from the Massachusetts Institute of Technology, Northeastern University, the NOAA-Northeast Fisheries Science Center, the Naval Research Laboratory, Penn State University, and the Woods Hole Oceanographic Institution in the US, as well as the Institute of Marine Research-Bergen in Norway.

The GOME06 [12,13,32,33,56,57,60–62] was conducted from September 19–October 6, 2006, in conjunction with the US National Marine Fisheries Services (NMFS) annual Atlantic herring acoustic survey [63,64] of the Gulf of Maine and Georges Bank. The Atlantic herring areal population densities were monitored over instantaneous wide areas using ocean acoustic waveguide remote sensing (OAWRS) imaging [12,13,33,56,62] and calibrated with coincident conventional ultrasonic fisheries echosounding measurements [65]. The RV Delaware II conducted the ultrasonic fisheries echosounding survey and trawl sampling to enable fish species identification and fish physiological parameters to be extracted from the trawl samples collected over the course of the experiment [65]. The NorEx14 was conducted from February 18– March 7, 2014, in conjunction with Norway's Institute of Marine Research (IMR) survey of the fish populations of the Norwegian Sea. Both the RV Johan Hjort and the FV Artus conducted ultrasonic fisheries echo sounding and trawl surveys of the fish populations.

In both GOME06 and NorEx14, recordings of underwater sound were acquired using a large-aperture densely-sampled horizontal coherent hydrophone array [66] towed along designated tracks for 8 to 24 h per day. To minimize the effect of tow ship noise on the recorded acoustic data, the coherent hydrophone array was towed approximately 375–405 m and 282–329 m behind the research vessel during GOME06 and NorEx14, respectively, so as to confine this noise to the forward end-fire direction of the array. The tow ship noise in directions away from the forward end-fire was negligible after coherent beamforming. The multiple nested sub-apertures of the array contain a total of 160 hydrophones spanning a frequency range from below 50 Hz to 3750 Hz for spatially unaliased sensing. A fixed sampling frequency of 8000 Hz was used so that acoustic signals with frequency contents up to 4000 Hz were recorded without temporal aliasing. Three linear nested sub-apertures of the array, the ultra low-frequency (ULF), mid-frequency (MF) and high-frequency (HF) sub-apertures, each consisting of 64 equally spaced hydrophones with inter-element spacings of 3 m, 0.75 m, and 0.375 m respectively, were used to analyze the ship-radiated sound with frequency content below 2000 Hz. The angular resolution or equivalent beamwidth $\beta(\phi, f_c)$ of each uniformly-spaced subaperture of the horizontal receiver array is $\beta(\phi, f_c) = 1.44(\lambda/L\cos\phi)$ for broadside $(\phi = 0)$ through angles near endfire $(\phi = \pi/2)$, where $\lambda = c/f_c$ is the acoustic wavelength, c is the sound speed, f_c is the center frequency, and L is the array subaperture length [33,56]. At endfire, the angular resolution is $\beta(\phi, f_c) \approx 2.8\sqrt{\lambda/L}$ [67]. The angular resolution of the receiver array is tabulated in Table 1 of [56] at selected frequencies for each uniformly-spaced sub-aperture. Note that the equivalent beamwidth is the angular width of a rectangular or uniform function that has the same receptivity as the array integrated over all azimuths. The water depth ranged from 180 to 250 m at the array locations

and the array tow depth was roughly 105 m in GOME06. The water depth ranged from 100 to 300 m at the array locations and the array tow depth was roughly 45–70 m in NorEx2014.

Physical oceanography was monitored in both experiments by sampling water-column temperature and salinity with expendable bathythermographs (XBTs) and conductivity-temperature-depth (CTD) sensors at regular hourly intervals. The water-column sound speed profile was found to be relatively constant in space and time over the experimental duration in GOME06, as shown by the compilation of over roughly 200 samples taken during the experiment in Figure 3 of [56] and Figure 2 of [57]. The sound speed profiles measured in the Norwegian Sea are provided in Appendix F Figures F2–F6 from [68].

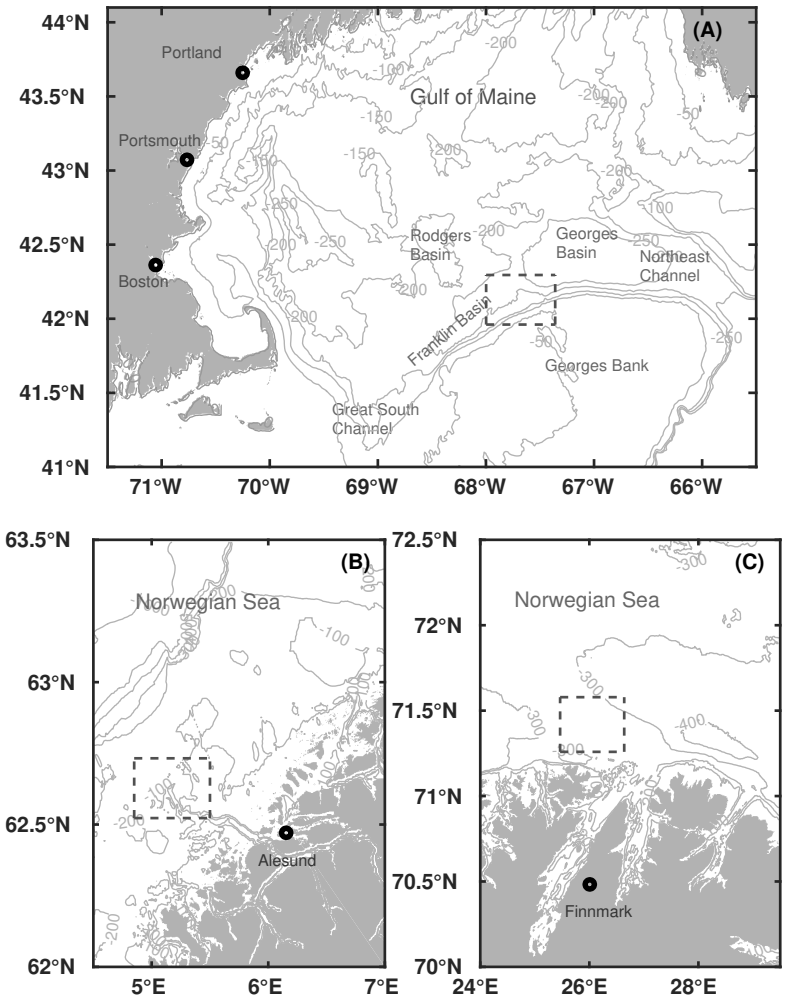

Figure 1. (**A**) Location of the US Gulf of Maine 2006 Experiment (GOME06) on October 3 on the northern flank of Georges Bank in the Gulf of Maine where the research vessel (RV) Delaware II was present. The gray dashed box bounds the area of Figure 4A. (**B**) Location of the Norwegian Sea 2014 Experiment (NorEx2014) on February 21 in the Norwegian Sea off Alesund where the fishing vessel (FV) Artus was present. The gray dashed box bounds the area of Figure 12A. (**C**) Location of NorEx2014 on March 3 in the Norwegian Sea off Finnmark where the RV Johan Hjort was present. The gray dashed box bounds the area of Figure 8A.

The detection of long-range propagated sounds is significantly enhanced by spatial beamforming and spectrogram analysis which filters the background noise that is outside of the beam and frequency

band of the ship-radiated sound. The high gain [69,70] of the large aperture densely-sampled coherent hydrophone array used here, roughly $10 \log_{10} n = 18$ dB gain with $n = 64$ hydrophones for each sub-aperture, enabled detection of continuous tonal noises either two orders of magnitude more distant in range or lower in SNR than a single hydrophone which has no array gain (see Figure 2).

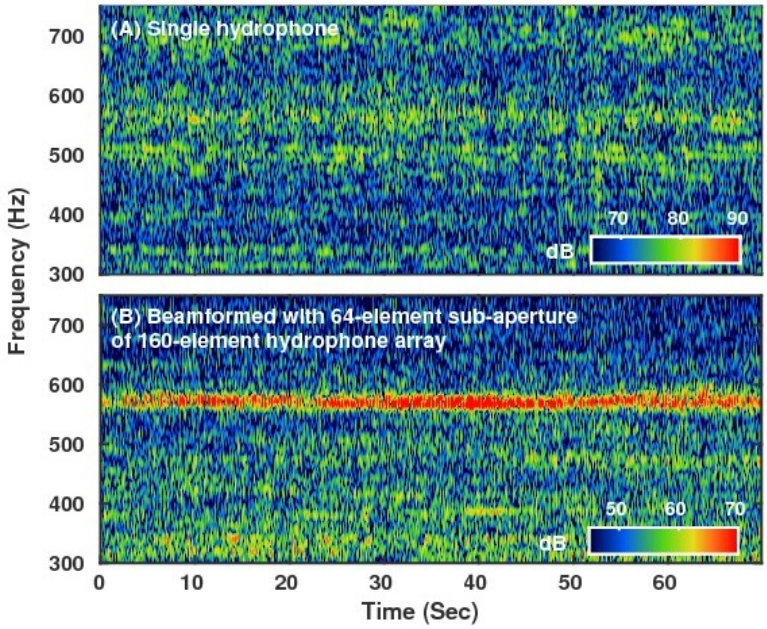

Figure 2. Coherent array processing enhances signal-to-noise ratio (SNR) for detection of ship sound. Compare single hydrophone measured spectrogram in (**A**) with spectrogram after coherent beamforming in (**B**) with 64-element MF subaperture of passive ocean acoustic waveguide remote sensing (POAWRS) 160-element hydrophone array. The narrowband tonal signal from the RV Delaware II roughly 23 km away from the POAWRS receiver array recorded on 3 October 2006 at 21:23:45 EDT is enhanced by 18 dB above the background noise after beamforming in (**B**) where the ship bearing is -45° from the array broadside.

The POAWRS coherent hydrophone array employed in GOME06 and NorEx14 detected significant sounds from a wide range of underwater acoustic sources including marine mammal vocalizations from diverse baleen and toothed whale species in the frequency range from 10 Hz up to 4 kHz [13,32,33,35]. Here the analysis is focused on the detection and characterization of the long range propagated sound radiated from the three known ships in the 10 Hz to 2000 Hz frequency range including overall broadband levels and narrowband tonals at discrete frequencies, so as to provide a calibration of the POAWRS approach for passive acoustic monitoring of surface ships.

2.2. Ship-Radiated Sound Detection, Bearing Estimation and Characterization

Acoustic pressure time series measured by sensors across the receiver array were converted to two-dimensional beam-time series by beamforming [70]. A total of 64 beams were formed spanning 360-degree horizontal azimuth about the receiver array for data from each subaperture. Each beam-time series was converted to a beamformed spectrogram by short-time Fourier transform (sampling frequency = 8000 Hz, frame = 2048 (ULF), 1024 (MF) and 516 (HF) samples, overlap = 15/16, Hann window). Significant sounds present in the beamformed spectrograms were automatically detected by first applying a pixel intensity threshold detector followed by pixel clustering, and verified by visual inspection. Beamformed spectrogram pixels with local intensity values that are 5.6 dB above the background are grouped using a clustering algorithm according to a nearest-neighbour criteria that determines if the pixels can be grouped into one or more significant sound signals. Each detected

signal is next characterized by its pitch track representing the time variation of the fundamental frequencies. The pitch track is estimated using a time-frequency peak detector from a signal's detected and clustered pixel intensity values in the beamformed spectrogram.

The horizontal azimuthal direction or bearing $\hat{\beta}$ of each detected signal, measured from the array broadside, is estimated using beamforming technique [70], by selecting the bearing in which the beamformed, bass-pass filtered pressure-time series contained maximum energy during the time duration of the signal and in the same frequency band. The estimated relative bearings $\hat{\beta}$ measured with respect to array broadside are then converted to absolute bearings, measured from the array center with respect to true North. The true bearings versus time trajectories of all of the signal detections for a given day of data collection are compared with the true bearings of the known research or fishing vessels present in the area, calculated from the GPS locations of each ship and the hydrophone array. Signal detections with bearing-time trajectories that coincide well with the bearing-time trajectory of each ship are further extracted and associated to that ship. The time-frequency characteristics of these extracted signals, determined from their pitch-tracks, are quantified for each ship analyzed here.

The pitch track for a signal contains a time series $t = (t_1, t_2, ..., t_i)$, a frequency series $f = (f_1, f_2, ..., f_i)$, and an amplitude series $A = (A_1, A_2, ..., A_i)$ describing the time-variation of the fundamental frequency in the signal [71,72]. Ten features are extracted from each signal. They are: (1) minimum frequency (Hz), f_{min}; (2) maximum frequency (Hz), f_{max}; (3) signal bandwidth (Hz), $\bar{B} = f_{max} - f_{min}$; (4) amplitude-weighted average slope (octaves per second), β; (5) amplitude-weighted average frequency ($\log_2$[Hz]), $\bar{f}$; (6) time variation (second), $\langle t \rangle$; (7) frequency variation ($log_2[Hz]$), $\langle f \rangle$; (8) duration (second), $\tau = t_i - t_1$; (9) slope from first order polynomial fit (degrees), β_{poly}; and (10) curvature from second-order polynomial fit, ν. The four amplitude-weighted features (4)–(7) are calculated using the formulation provided in Table 1 of [71]. As explained in [71], an advantage of characterizing signals with the amplitude-weighted attributes is that it provides a more consistent representation of a signal when data is noise-limited.

2.3. Source Level Estimation for Ship Tonal and Cyclostationary Signals

The source levels of the ship-radiated prominent narrowband tonals and cyclostationary signals at specific frequencies are determined following the approach described in Section 2.5 of [35] and Section 3.5 of [33]. The source level $SL(\mathbf{r_0})$ of each signal is estimated from its received pressure level $RL(\mathbf{r})$ via the passive sonar equation [9,33,35,73],

$$SL(\mathbf{r_0}) = RL(\mathbf{r}) + TL(|\mathbf{r} - \mathbf{r_0}|). \quad (1)$$

The received pressure level is estimated as the peak value of the instantaneous time-domain signal bandpass filtered within a bandwidth $(f_U - f_L)$ that is 3-dB down on both sides of the spectral peak for a given prominent tonal or cyclostationary signal. The corresponding one-way acoustic transmission loss $TL(|\mathbf{r} - \mathbf{r_0}|)$ from the ship location to the center of the POAWRS receiver array is calculated using a calibrated [56,57] parabolic equation-based range-dependent acoustic propagation model (RAM) [58,59] via [54–57],

$$\mathrm{TL}(|\mathbf{r} - \mathbf{r_0}|) = -10 \log_{10} \left(\int_{f_L}^{f_U} Q(f) \langle |G(\mathbf{r}|\mathbf{r_0}, f)|^2 \rangle df \right), \quad (2)$$

where $G(\mathbf{r}|\mathbf{r_0}, f)$ is the waveguide Green function at frequency f for ship located at $\mathbf{r_0}$ and receiver array center at $\mathbf{r}$, $Q(f)$ is the normalized spectra of ship tonal or cyclostationary signal, and f_U and f_L are the upper and lower frequencies used in the bandpass filter. The model takes into account the environmental parameters such as the range-dependent water depth and sound speed profiles to stochastically compute the propagated acoustic intensities via Monte-Carlo simulations following the approach of [54–56]. The range- and depth-dependent acoustic transmission loss is plotted for transects in the Gulf of Maine in Figure 4 of [57] and in the Norwegian Sea in Figures 5 and 6 of [68]. The mean

magnitude-squared waveguide Green function is obtained by averaging over multiple depths for each ship from the sea surface to the ship draft depth or draught z_{draft} and over multiple Monte-Carlo simulations to account for waveguide fluctuations. The draught used here are $z_{draft} = 4.5$ m for RV Delaware II, $z_{draft} = 6.5$ m for RV Johan Hjort, and $z_{draft} = 6$ m for FV Artus.

The stochastic broadband transmission loss model calculations have been extensively calibrated and verified with: (1) thousands of one-way transmission loss measurements made during the same GOME06 experiment discussed here at the same time and at the same location [56,57]; (2) thousands of two-way transmission loss measurements made from herring shoal returns and verified by conventional fish finding sonar and ground truth trawl surveys during the same GOME06 experiment discussed here at the same time and at the same location [12,56,64]; (3) roughly 100 two-way transmission loss measurements made from calibrated targets with known scattering properties during the same GOME06 experiment discussed here at the same time and at the same location [61]; and (4) thousands of one-way transmission loss measurements made during a past POAWRS experiment conducted in a similar continental shelf environment [54]. Calibration of the stochastic broadband transmission loss model for the Norwegians Sea is provided in [68]. The source level results are provided in units of dB re 1 μPa/Hz at 1 m so that they can be compared to the results in the literature.

2.4. Probability of Detection Regions for Prominent Ship-Radiated Signals

The probability of detection (POD) regions for the prominent tonals or cyclostationary signals radiated from each of the research and fishing vessels considered here and received on the coherent hydrophone array are calculated using the approach provided in Appendix A. We model the POD regions for RV Delaware II in the Gulf of Maine, and RV Johan Hjort and FV Artus in the Norwegian Sea.

3. Results

Here we first associate the acoustic signal detections in the 10 Hz to 2000 Hz frequency range measured by the coherent hydrophone array with the known ships since they occur in bearing-time trajectories that coincide with those of the ships the RV Delaware II in the Gulf of Maine, and the FV Artus and RV Johan Hjort in the Norwegian Sea. We then provide a statistical time-frequency characterization of the detected signals associated with each ship. We find that the sounds radiated by the ships and received on the coherent hydrophone array after long-range propagation (4 km to 32 km range) are dominated by distinct narrowband tonals and/or cyclostationary signals in the 100 to 2000 Hz frequency range. We estimate the source level distributions of the prominent tonal and cyclostationary signals radiated by each ship. These results are then applied to estimate the probability of detection regions for the ship-radiated signals in the ocean environment where the measurements were made for each ship. Finally, we investigate the dependence on ship speed of the ship-radiated sound spectra and source level.

3.1. RV Delaware II

The bearing and time of all detected acoustic narrowband signals in the 200–1000 Hz frequency range, that stand at least 5.6 dB above the local ambient background noise, in the beamformed spectrograms of the coherent hydrophone array on October 3, 2006 during GOME06 when the RV Delaware II was present are shown in Figure 3A. The bearings of RV Delaware II as a function of time are also overlain for comparison. Detected signals in bearing-time trajectories that exactly coincide with the bearing-time trajectory of RV Delaware II (see Figure 3) are extracted and associated with RV Delaware II. The same procedure is applied to extract the signal detections associated with RV Delaware II in other frequency subbands, 10–200 Hz and 1000–2000 Hz.

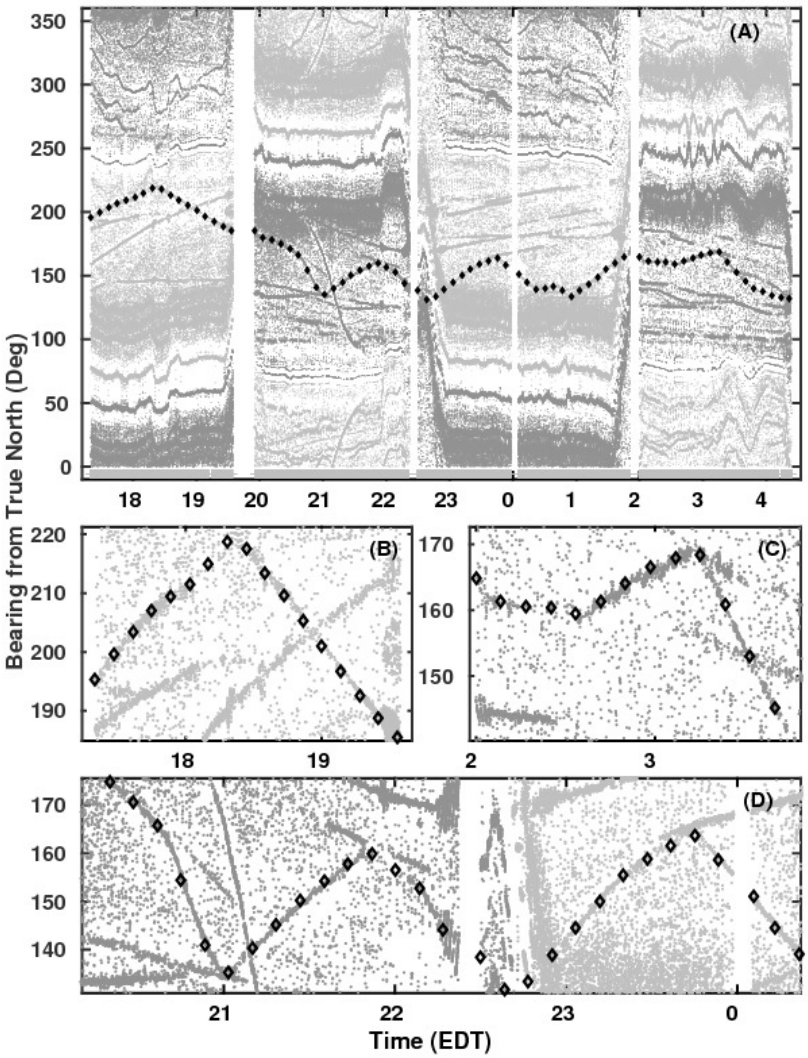

Figure 3. Extracting ship-radiated signals from the RV Delaware II. (**A**) Bearing and time of all detected signals on October 3 during GOME2006 in the 200–1000 Hz frequency range, spanning a 360-degree horizontal azimuth about the coherent hydrophone array from true north. Light and dark gray dots correspond to right and left side bearings respectively for all detections about the receiver array, before the line array's left-right bearing ambiguity resolution [60]. The black diamonds are the exact bearings of the RV Delaware II calculated from global positioning system (GPS)-measured locations of the RV Delaware II and coherent hydrophone array. The light gray bar at the bottom shows the coherent hydrophone array recording time intervals. (**B**–**D**) Enlarged figures show the tracking details in the three time periods: 17:10 to 19:40, 02:00 to 03:50 and 20:10 to 00:25 EDT. Detected signals within bearing-time trajectories that coincide with the bearing of the RV Delaware II are extracted and associated with RV Delaware II.

The tow tracks of the coherent hydrophone array and the corresponding locations of RV Delaware II on October 3, 2006 in the Gulf of Maine during GOME06 based on GPS measurements are shown in Figure 4A. The bearing-time trajectories of detected signals measured by the coherent hydrophone array that are associated with RV Delaware II in the three frequency subbands: 10–200 Hz, 200–1000 Hz and 1000–2000 Hz are plotted in Figure 4B–D.

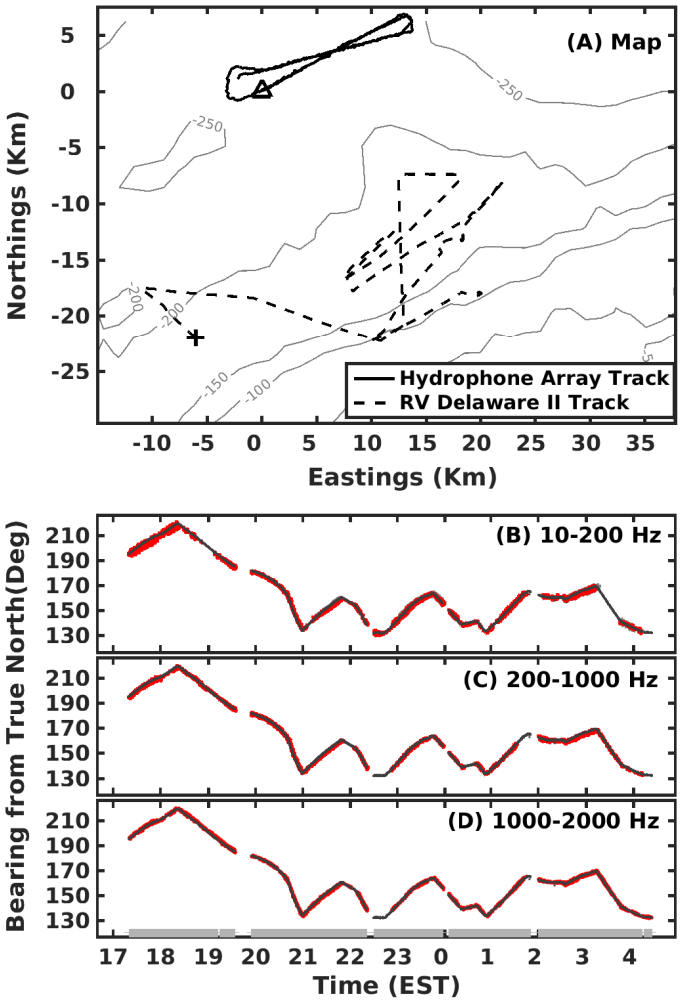

Figure 4. (**A**) Locations of the RV Delaware II and tow track of coherent hydrophone array during GOME2006 over the time period shown in Figure 3A. The origin of the coordinate system is the starting location of the coherent hydrophone array track indicated by the black triangle. The black plus indicates the starting location of the RV Delaware II. (**B**–**D**) Bearing and time of signal detections (red dots) on the coherent hydrophone array that are associated with the RV Delaware II (bearing shown in black) in the three frequency subbands shown. There are a total of 5550, 6570, and 112,230 signal detections in the 10–200 Hz, 200–1000 Hz and 1000–2000 Hz frequency bands respectively over the 11 h observation duration analyzed here.

The time-frequency characteristics of the detected signals associated with the RV Delaware II in the three frequency subbands are shown in Figure 5. The sound radiated by the RV Delaware II is dominated by two distinct narrowband tonals at roughly 176 Hz and 573 Hz Examples of beamformed spectrograms containing these two distinct tonals, as well as other broadband and narrowband signals associated with RV Delaware II are shown in Figure 5A–C. The ensemble of pitch tracks and the histogram of mean frequency weighted by signal duration for the ship-associated detections in the three frequency subbands are shown in Figure 5D–I.

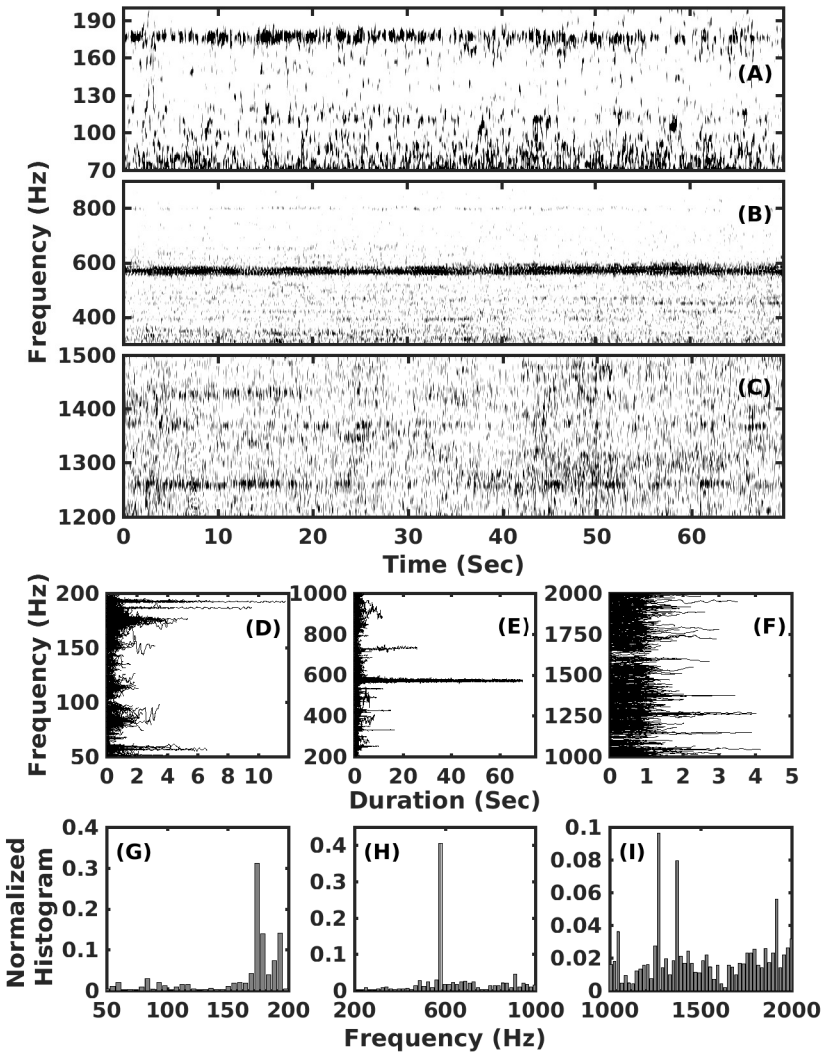

Figure 5. Characteristics of signal detections associated with the RV Delaware II during GOME2006. (**A**–**C**) Examples of beamformed spectrograms containing prominent narrowband tonals and less prominent broadband signals; (**D**–**F**) The ensemble of pitch tracks of the signal detections in the 10–200 Hz, 200–1000 Hz and 1000–2000 Hz frequency ranges; (**G**–**I**) The normalized histogram of center frequency weighted by the signal duration for the signal detections associated with the RV Delaware II.

The source level distributions for the ship-radiated tonals at 176 Hz and 573 Hz are determined from a subset of the measured signals (see Figure 6) on the coherent hydrophone array. The mean and standard deviation of the source level in units of dB re 1 µPa/Hz at 1 m for the tones at 176 Hz and 573 Hz are 148.7 $\pm$ 5.2 and 162.3 $\pm$ 6.0, respectively, with 3 dB-down instantaneous bandwidths of 3.5 Hz and 0.8 Hz, respectively.

The POD regions for the tonal sound at 176 Hz and 573 Hz radiated by RV Delaware II and received by the coherent hydrophone array in the Gulf of Maine environment are shown in Figure 7. The 50% POD region extends over an area measuring between 100 km to 200 km diameter. The POD region is significantly larger for the 573-Hz tonal sound radiated by the RV Delaware II than for the 176 Hz tonal. This is because the 573-Hz tone is radiated with a roughly 14-dB higher source level than the 176-Hz tone and the background ambient noise level is lower at 573 Hz than at 176 Hz by 5.2 dB. The 176 Hz tone has a slightly larger bandwidth of 3.5 Hz compared to 0.8 Hz for the 573 Hz tone. In contrast, the 50% POD region for tonal detection using a single hydrophone at each of the center locations of the coherent hydrophone array is significantly smaller (see dashed curve in Figure 7).

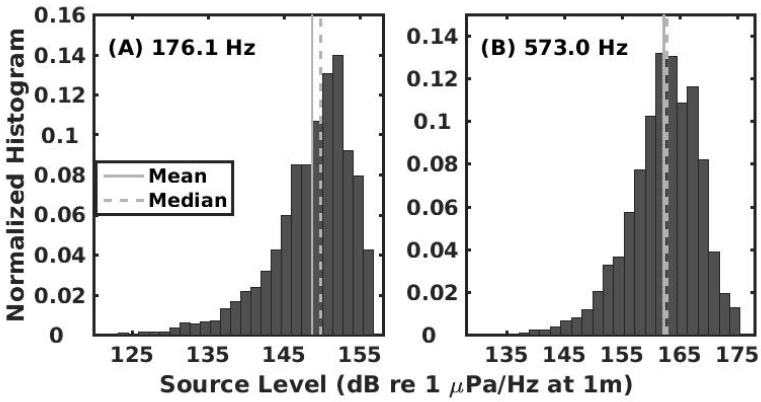

Figure 6. Normalized histogram of the estimated source levels of the narrowband tonal signals centered at (**A**) 176 Hz and (**B**) 573 Hz associated with the RV Delaware II during GOME06. Roughly 162,680 and 3,132,700 independent estimates of the instantaneous source level are used to generate the histograms in (**A**,**B**), respectively.

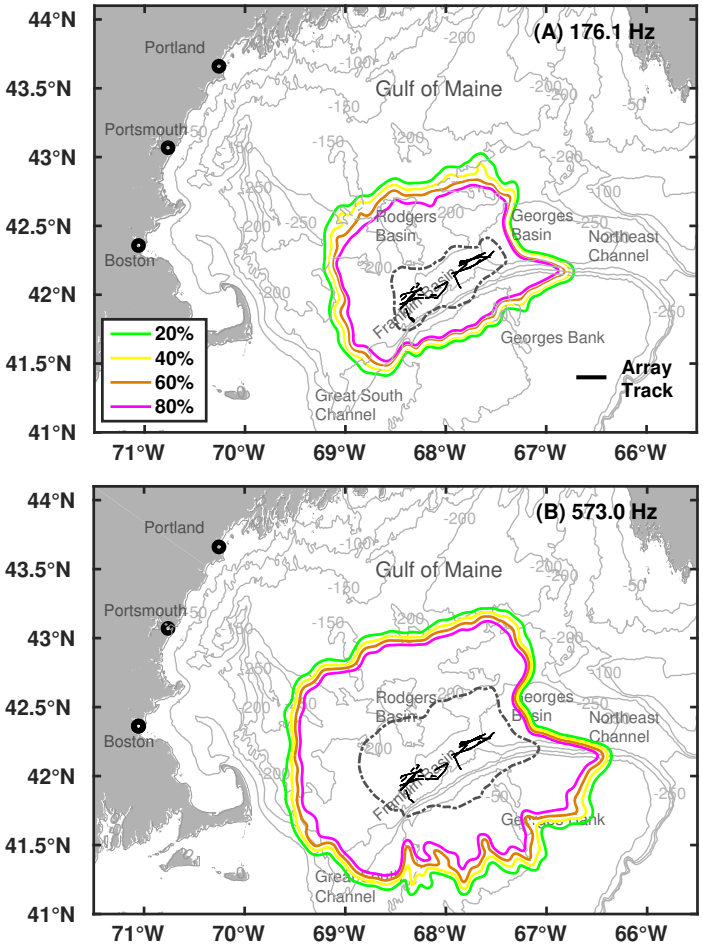

Figure 7. Probability of detection regions for the narrowband tonal signals centered at (**A**) 176 Hz and (**B**) 573 Hz radiated by the RV Delaware II and received on the coherent hydrophone array. The gray dash curves are the 50% probability of detection regions for corresponding signal receptions on a single hydrophone located at each of the center location of the coherent hydrophone array.

3.2. RV Johan Hjort

The tow tracks of the coherent hydrophone array and the corresponding locations of RV Johan Hjort on March 3, 2014 in the Norwegian Sea during NorEx14 based on GPS measurements are shown in Figure 8A. The bearing-time trajectories of detected signals measured by the coherent hydrophone array that are associated with the RV Johan Hjort in the three frequency subbands: 10–200 Hz, 200–1000 Hz and 1000–2000 Hz are plotted in Figure 8B–D.

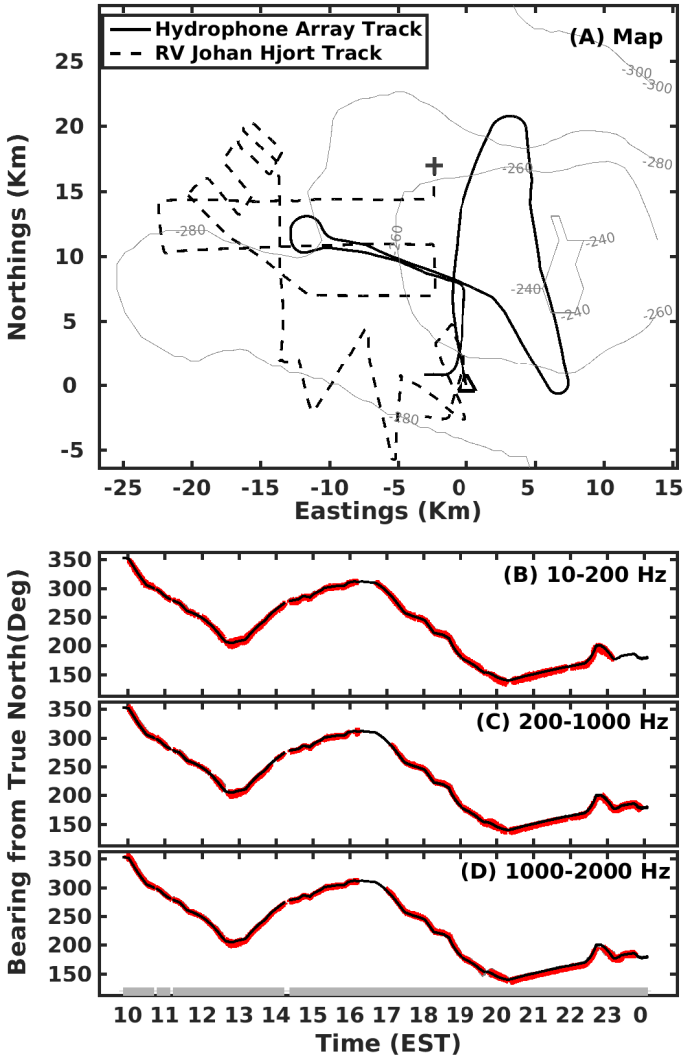

Figure 8. (**A**–**D**) Locations of the RV Johan Hjort and the tow track of coherent hydrophone array during NorEx2014 on March 3. The origin of the coordinate system is the starting location of the coherent hydrophone array track indicated by the black triangle. The black plus indicates the starting location of RV Johan Hjort. (**B**–**D**) Bearing and time of signal detections (red dots) on the coherent hydrophone array that are associated with the RV Johan Hjort (bearing shown in black) in the three frequency subbands shown. There are a total of 11,500, 18,000 and 23,600 signal detections in the 10–200 Hz, 200–1000 Hz and 1000–2000 Hz frequency bands, respectively, over the 14-h observation duration analyzed here.

The time-frequency characteristics of the detected signals associated with the RV Johan Hjort in the three frequency subbands are shown in Figure 9. The sound radiated by RV Johan Hjort is dominated by three distinct narrowband tonals centered at 168.5 Hz, 694 Hz and 808 Hz. Examples of

beamformed spectrograms containing these tonal signals, as well as other broadband and narrowband signals associated with the RV Johan Hjort are shown in Figure 9A–C. The ensemble of pitch tracks and the histogram of mean frequency weighted by signal duration for the ship-associated detections in the three frequency subbands are shown in Figure 9D–I.

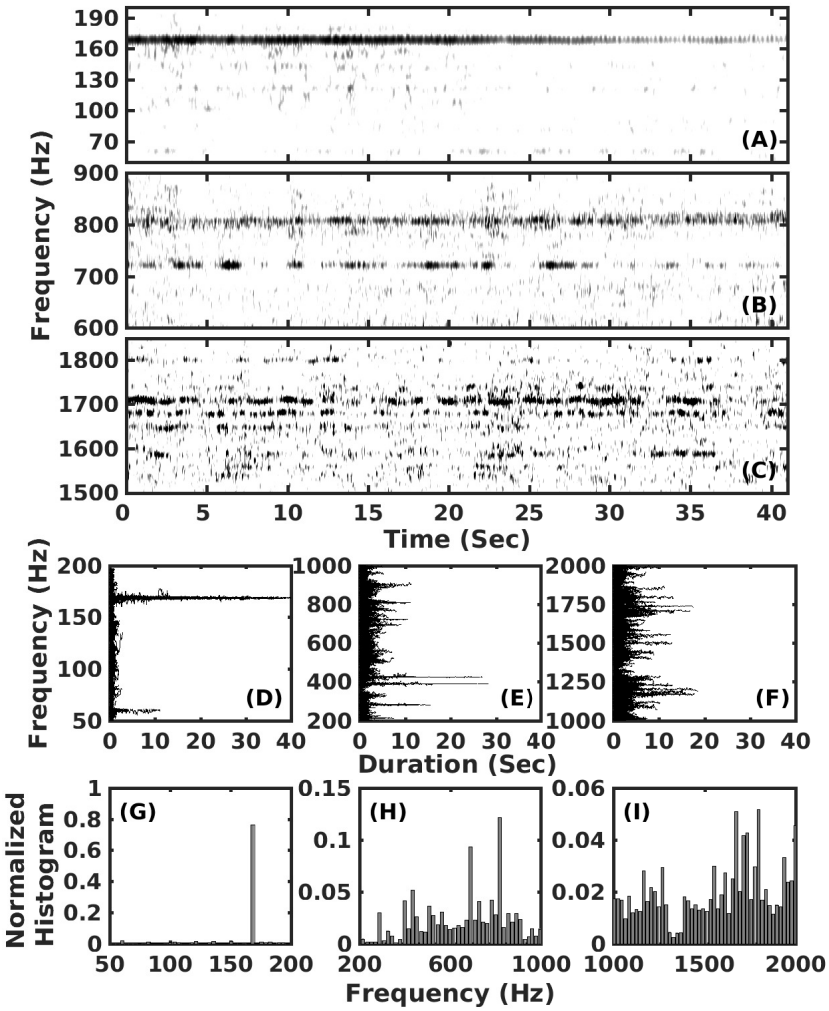

Figure 9. Characteristics of signal detections associated with the RV Johan Hjort during NorEx2014. (**A**–**C**) Examples of beamformed spectrograms containing prominent narrowband tonals and less prominent broadband signals; (**D**–**F**) The ensemble of pitch tracks of the signal detections in the 10–200 Hz, 200–1000 Hz and 1000–2000 Hz frequency ranges; (**G**–**I**) The normalized histogram of center frequency weighted by the signal duration for the signal detections associated with the RV Johan Hjort.

The source level distributions for the ship-radiated tonal signals centered at 168.5 Hz, 694 Hz, and 808 Hz are determined from a subset of the measured signals (see Figure 10) on the coherent hydrophone array. The mean and standard deviation of the source level in units of dB re 1 µPa/Hz at 1 m for the tonal signals centered at 168.5 Hz, 694 Hz and 808 Hz are 168.4 $\pm$ 7.2, 147.6 $\pm$ 4.3 and 148.5 $\pm$ 4.0 dB, respectively, with three dB-down instantaneous bandwidths of 0.8 Hz, 3 Hz and 2 Hz, respectively.

The POD regions for the tonal signals centered at 168.5 Hz, 694 Hz and 808 Hz radiated by the RV Johan Hjort in the Norwegian Sea environment are shown in Figure 11. The 50% POD region extends over an area with a 100 km to 200 km diameter. The POD region is the largest for the 168.5 Hz tonal signal in comparison to that at the other frequencies.

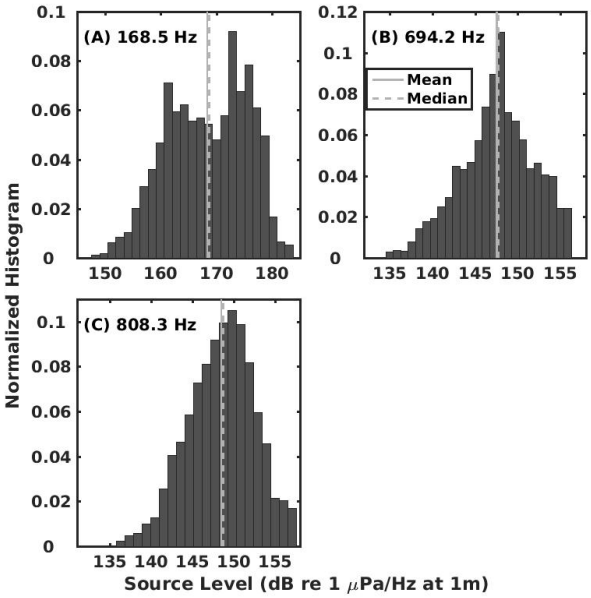

Figure 10. Normalized histogram of the estimated source levels of the narrowband tonal signals centered at (**A**) 168.5 Hz, (**B**) 694.2 Hz and (**C**) 808.3 Hz associated with the RV Johan Hjort during NorEx2014. Roughly 3,115,200, 288,000 and 1,219,300 independent estimates of the instantaneous source level are used to generate the histograms in (**A**–**C**), respectively.

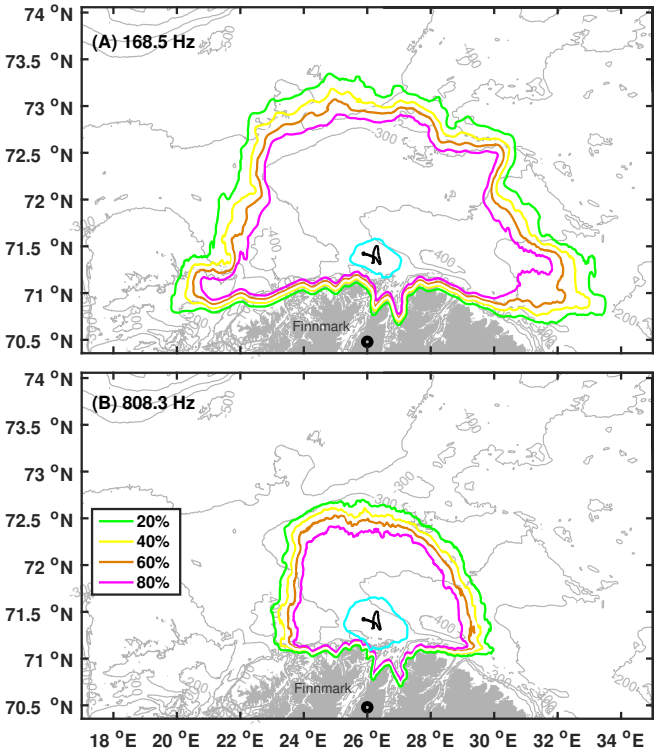

Figure 11. Probability of detection regions for the narrowband tonal signals centered at (**A**) 168.5 Hz and (**B**) 808 Hz radiated by the RV Johan Hjort and received on the coherent hydrophone array based on source level estimates here. In contrast, the POD regions (50%, cyan curve) are much smaller when the calculations are based on the lower one-third octave bandwidth intensity averaged source levels at around 168.5 Hz and 808 Hz with values of 142 and 133 dB re 1 μPa/Hz at 1 m respectively estimated from Figure 2 in [23].

3.3. FV Artus

The tow tracks of the coherent hydrophone array and the corresponding locations of the FV Artus on February 21, 2014 in the Norwegian Sea during NorEx14 based on GPS measurements are shown in Figure 12A. The bearing-time trajectories of signal detections measured by the coherent hydrophone array that are associated with the FV Artus in the three frequency subbands 10–200 Hz, 200–1000 Hz and 1000–2000 Hz are plotted in Figure 12B–D.

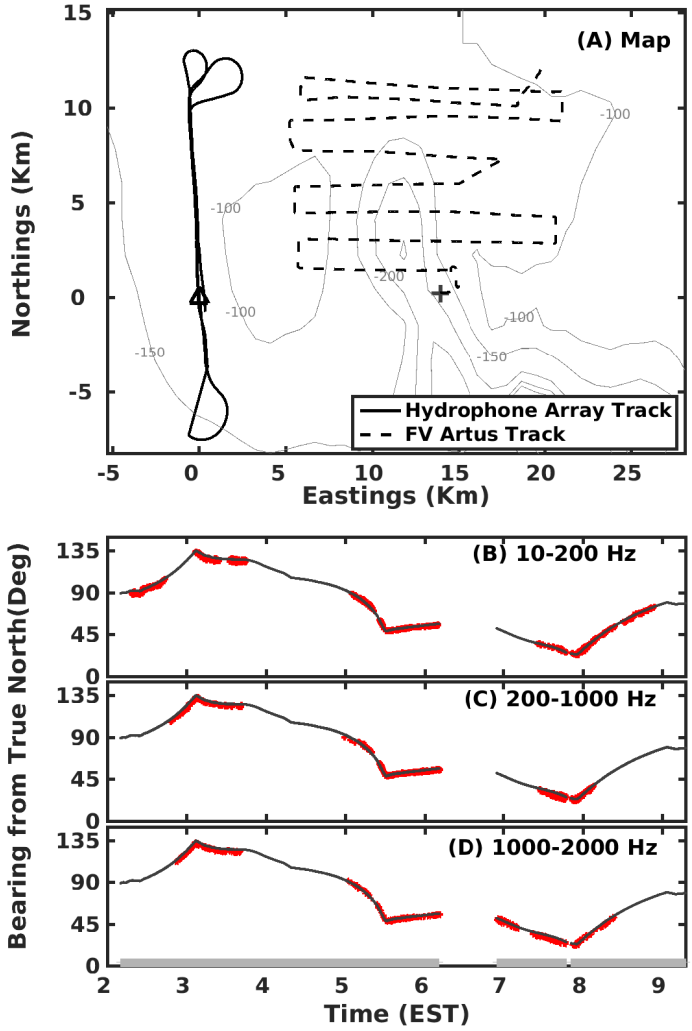

Figure 12. (**A**) Locations of the FV Artus and tow track of coherent hydrophone array during NorEx2014 on February 21. The origin of the coordinate system is the starting location of the coherent hydrophone array track indicated by the black triangle. The black plus indicates the starting location of the FV Artus. (**B**–**D**) Bearing and time of signal detections (red dots) on the coherent hydrophone array that are associated with FV Artus (bearing shown in black) in the three frequency subbands shown. There are a total of 2500, 2130 and 1640 signal detections in the 10–200 Hz, 200–1000 Hz and 1000–2000 Hz frequency bands respectively over the 6-h observation duration analyzed here.

The time-frequency characteristics of the detected signals associated with FV Artus in the three frequency subbands are shown in Figure 13. The sound radiated by FV Artus is dominated by four distinct cyclostationary signals centered at roughly 170 Hz, 716 Hz, 1584 Hz and 1791 Hz. Examples of beamformed spectrograms containing these four cyclostationary signals, as well as other broadband and narrowband signals associated with the FV Artus are shown in Figure 13A–C. The ensemble of

pitch tracks and the histogram of mean frequency weighted by signal duration for the ship-associated detections in the three frequency subbands are shown in Figure 13D–I.

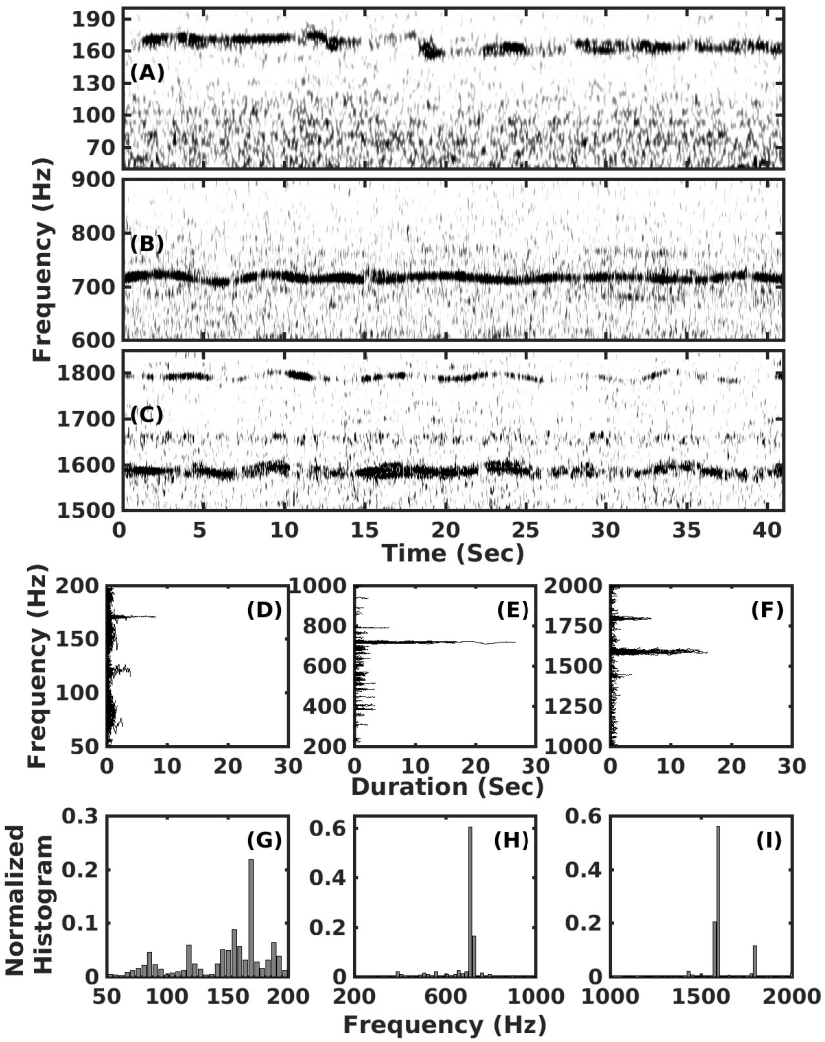

Figure 13. Characteristics of signal detections associated with the FV Artus during NorEx2014. (**A**–**C**) Examples of beamformed spectrograms containing prominent narrowband tonals and less prominent broadband signals. (**D**–**F**) The ensemble of pitch tracks of the signal detections in the 10–200 Hz, 200–1000 Hz and 1000–2000 Hz frequency ranges. (**G**–**I**) The normalized histogram of center frequency weighted by the signal duration for the signal detections associated with the FV Artus.

The source level distributions for the ship-radiated cyclostationary signals centered at 170 Hz, 716 Hz, 1584 Hz, and 1791 Hz are determined from a subset of the measured signals (see Figure 14) on the coherent hydrophone array. The mean and standard deviation of the source level in units of dB re 1 μPa/Hz at 1 m for the cyclostationary signals centered at 170 Hz, 716 Hz, 1584 Hz and 1791 Hz are 148.7 $\pm$ 2.1, 143.5 $\pm$ 5.8, 133.5 $\pm$ 6.0, and 130.0 $\pm$ 5.2 respectively, with 3 dB-down instantaneous bandwidths of 1.3 Hz, 2.5 Hz, 3.4 Hz, and 4 Hz, respectively.

The POD regions for the cyclostationary signals centered at 170 Hz, 716 Hz, and 1584 Hz radiated by the FV Artus and received by the coherent hydrophone array in the Norwegian Sea environment are shown in Figure 15. The 50% POD region extends over an area with between 100 km to 200 km diameter. The POD region is the largest for the 716 Hz cyclostationary signal in comparison to that at the other frequencies.

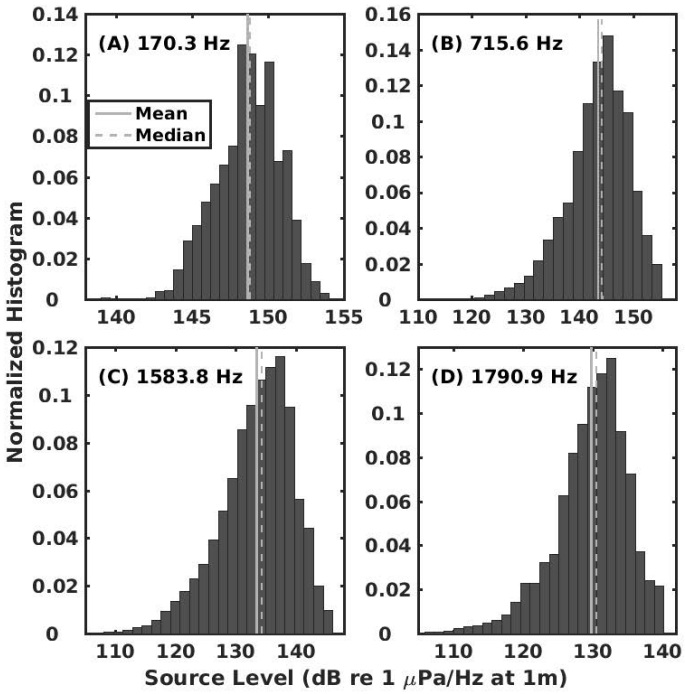

Figure 14. Normalized histogram of the estimated source levels of the narrowband tonal signals centered at (**A**) 170 Hz, (**B**) 716 Hz, (**C**) 1584 Hz and (**D**) 1791 Hz associated with FV Artus during NorEx2014. Roughly 267,300, 1,914,100, 1,576,100 and 440,400 independent estimates of the instantaneous source level are used to generate the histograms in (**A**–**D**), respectively.

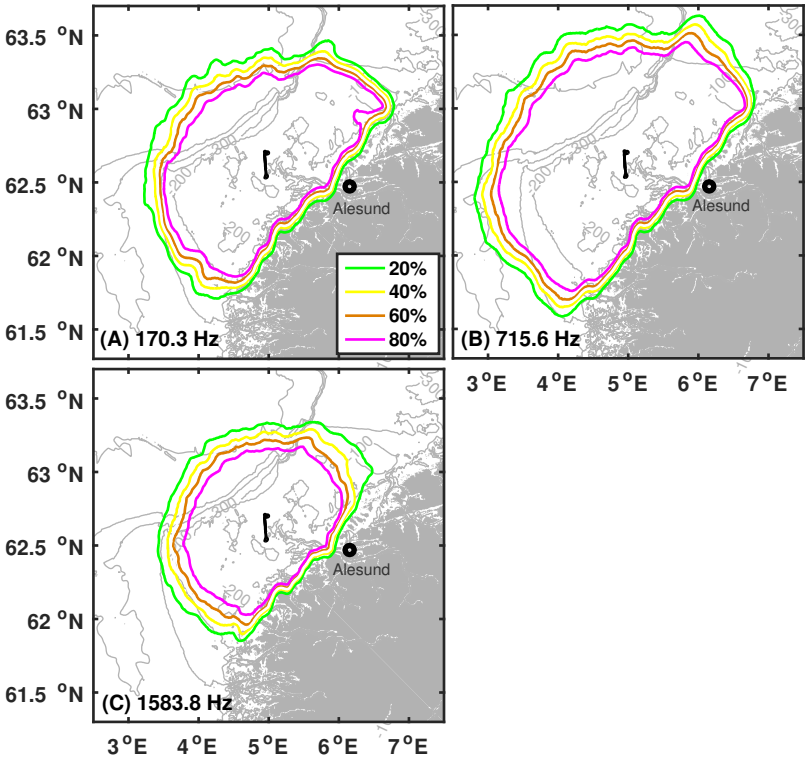

Figure 15. Probability of detection regions for the narrowband cyclostationary signals centered at (**A**) 170 Hz, (**B**) 716 Hz, (**C**) 1584 Hz and 1791 Hz radiated by the FV Artus and received on the coherent hydrophone array.

The prominent signals radiated by FV Artus have frequencies that are periodically oscillating about a mean value (see Figure 13). These signals can be modelled as cyclostationary random processes [74]. The frequency variation with time of the prominent cyclostationary signals can be approximated as,

$$f = f_0 + B\sin[2\pi\nu_1(t - t_0)] \quad (3)$$

where f_0 is the mean frequency, B is the amplitude of the frequency oscillation, and $\nu_1 = 1/\tau_1$, where τ_1 is the period of the frequency oscillations. Estimates of f_0, ν_1 and B for the three cyclostationary signals centered at 716 Hz, 1584 Hz and 1791 Hz radiated by FV Artus are provided in Table 1 and plotted in Figure 16. The period of the frequency oscillations is roughly $\tau_1 \approx 6.3$ s.

Table 1. Parameters used in Equation (3) to model the frequency oscillations of the narrowband cyclostationary acoustic signals radiated by the FV Artus.

f_0 (Hz)	B (Hz)	ν_1 (Hz)
715.6	9.3	0.15
1583.8	8.0	0.16
1790.9	8.3	0.164

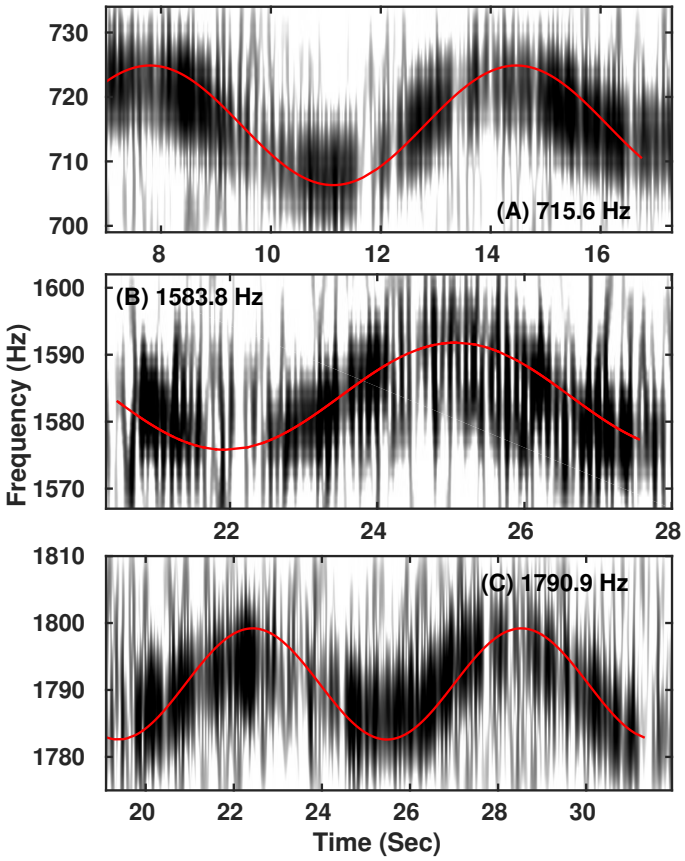

Figure 16. (**A**–**C**) Narrowband cyclostationary signals radiated by the FV Artus have cyclical frequency variations occurring over a period of roughly 6.3 s that can be modelled (black curve) using Equation (3).

3.4. Dependence of Ship-Radiated Sound on Ship Speed

The histogram of ship speed over the analysis time period for each of the three vessels are plotted in Figure 17. The ship speed is broadly distributed with multiple local peaks spanning stationary

0 m/s to fast moving at 18 m/s for the RV Delaware II. The ship speed is relatively consistent and centered at roughly 4 m/s for FV Artus. The speed of the RV Johan Hjort is bimodal and centered at roughly 1 m/s and 5 m/s.

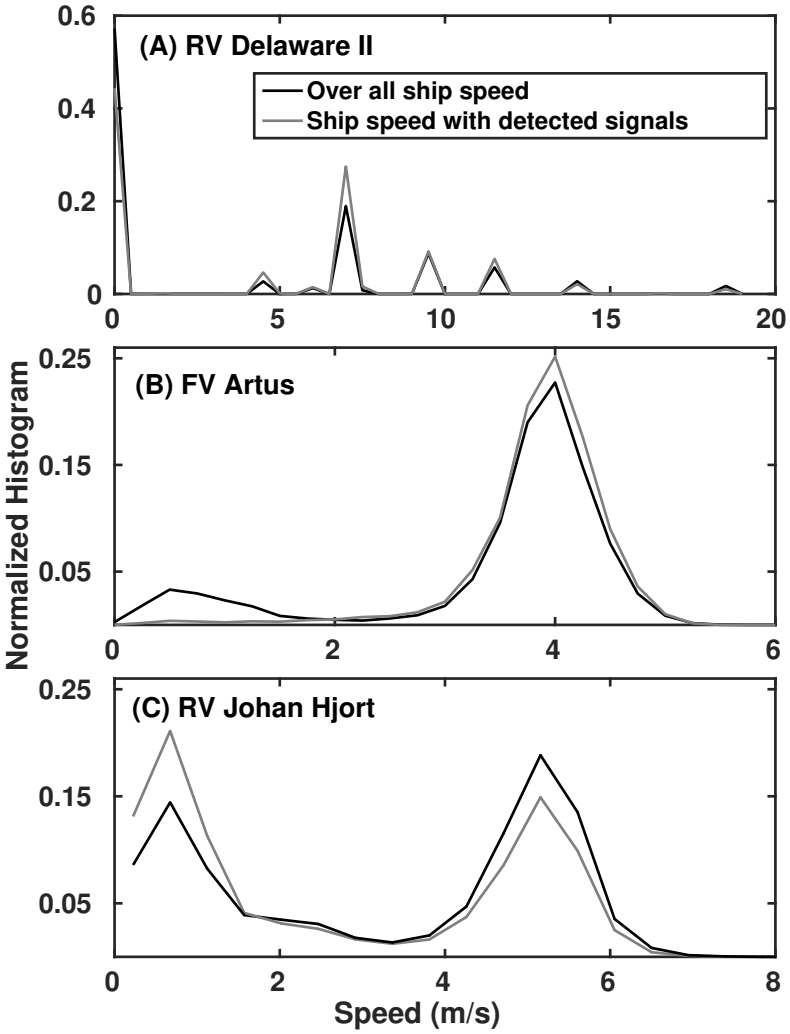

Figure 17. Normalized histogram of ship speed over the analysis duration presented here for (**A**) the RV Delaware II, (**B**) the FV Artus, and (**C**) the RV Johan Hjort.

Here we examine the source level and spectra of signal detections for the RV Johan Hjort as a function of two ship speed ranges, $\leq$2 m/s and 4–6 m/s. At low ship speed $\leq$2 m/s, the mean frequency of detected signals is more broadly distributed (Figure 18A) with the dominant tonal at 168.5 Hz emitted with more consistent source level, since its source level distribution is peakier with smaller standard deviation (Figure 19). Furthermore, the higher frequency tonals at 694 Hz and 808 Hz are negligible. At higher ship speed 4–6 m/s, the sound emitted is dominant by multiple tones, including the ones 168.5 Hz, 694 Hz and 808 Hz. The dominant tonal at 168.5 is emitted with more broadly distributed source level (Figure 19).

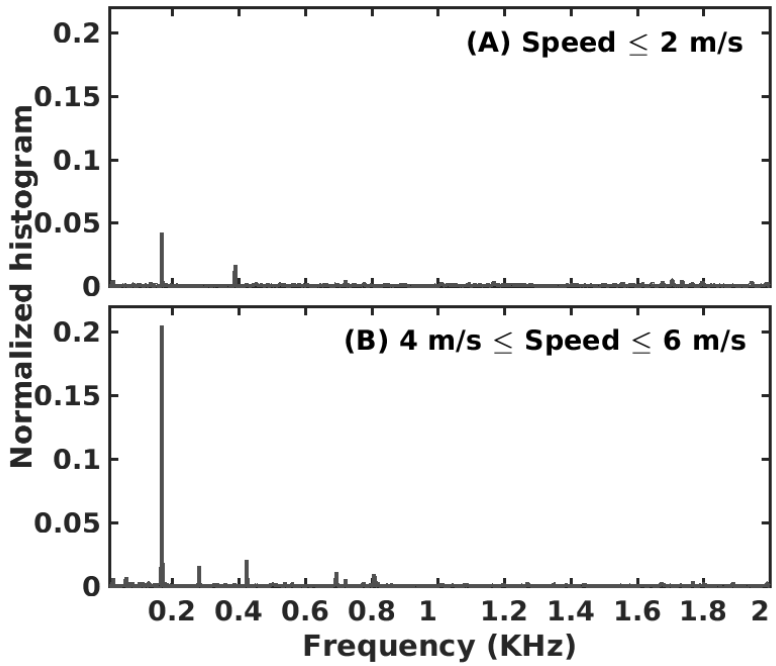

Figure 18. The normalized histogram of center frequency weighted by the signal duration for the signal detections associated with the RV Johan Hjort during NorEx2014 as a function of ship speed. (**A**) Ship speed ≤2 m/s. (**B**) 4 m/s ≤ Ship speed ≤6 m/s.

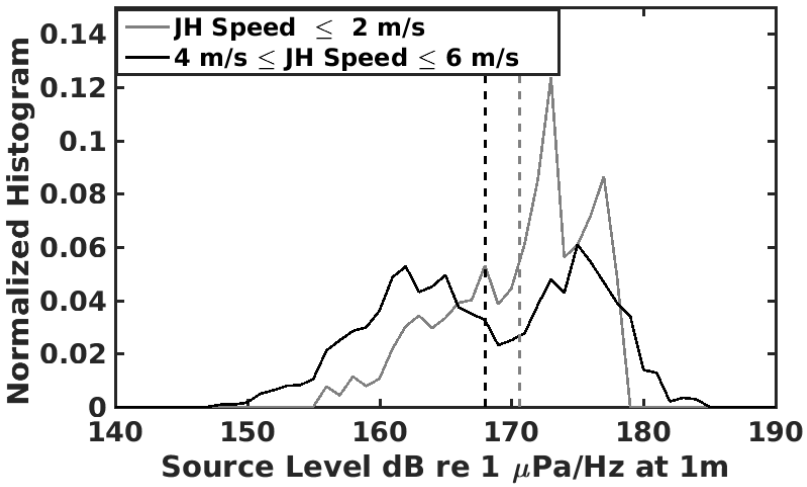

Figure 19. Normalized histogram of the estimated source levels of the narrowband tonal signals centered at 168.5 Hz, radiated by the RV Johan Hjort during NorEx2014 as a function of ship speed.

4. Discussion Including Implications for Studies of Vessel-Induced Fish Behavior

The ship-radiated sound received on the coherent hydrophone array after long range propagation (4–32 km) from all three research and fisheries survey vessels investigated here: the RV Delaware II, the RV Johan Hjort and the FV Artus; are dominated by narrowband tonals or cyclostationary signals that occur in the frequency range from 150 Hz to 2000 Hz. The lower frequency tonals around 170 Hz radiated from each ship are probably excited by internal machinery of the ship, such as motor and gear assembly, and then radiated through the hull [41]. The higher frequency tonals and cyclostationary signals in the 500 Hz to 2000 Hz range may be "propeller singing" resulting from fluid–structure interaction at the trailing edges of the propeller blades [75] (see Figure 1 of [41]).

The published spectra of ship-radiated sound from RV Johan Hjort are presented as one-third octave bandwidth intensity-averaged levels in the 10 Hz to 10 kHz frequency range in [23,28]. In [23], the results of which are reproduced in [22,30], the one-third octave bandwidth intensity averaged source levels of the RV Johan Hjort in units of dB re 1 µPa/Hz at 1 m in the 100 Hz to 1000 Hz frequency range at ship speed of 11 knots lie in the 134 to 142 dB range (see Figure 2 of [23]). In the same reference [23], it is also shown that the underwater sound radiated from RV Johan Hjort is highly dynamic where the one-third octave bandwidth intensity averaged source level can increase by 20 dB with changes in ship conditions such as ship speed and machinery propeller pitch and shaft speed. In [28], the one-third octave bandwidth-averaged source levels of RV Johan Hjort in units of dB re 1 µPa/Hz at 1 m in the 100 Hz to 1000 Hz frequency range from 125 dB to 150 dB with local peaks near 170 Hz, 320 Hz and 500 Hz with levels of 150 dB, 142 dB and 138 dB, respectively (see Figure 13 of [28]).

The source level of the dominant tonals found here for RV Johan Hjort based on measurements with the coherent hydrophone array in 2014 are 168.4 $\pm$ 6 at 168.5 $\pm$ 0.8 Hz, 147.6 $\pm$ 6 at 694 $\pm$ 3 Hz and 148.5 $\pm$ 6 at 808 $\pm$ 2 Hz in units of dB re 1 µPa/Hz at 1 m. The 168.5 $\pm$ 0.8 Hz tonal found here lies within the one-third octave band with corner frequencies of 140.3 Hz and 176.8 Hz, and bandwidth of 36.5 Hz. This tonal contribution can get reduced by up to $10\log_{10}(36.5/0.8) \approx 16.5$ dB after on third-octave bandwidth averaging, providing a closer match to the 170 Hz level of 150 dB re 1 µPa/Hz at 1 m found in [28]. The 694 $\pm$ 3 Hz tonal found here lies within the one-third octave band with corner frequencies of 561.2 Hz and 707.1 Hz, and bandwidth of 145.9 Hz. This tonal contribution can get reduced by up to $10\log_{10}(145.9/3) \approx 16.8$ dB after one-third octave bandwidth averaging. For both frequency bands, the overall one-third octave bandwidth averaged level will include intensity contributions from broadband signals present in the bandwidth, in addition to the tonals. In conclusion, the sound radiated by a ship underwater and received at long ranges can vary significantly with ship conditions such as ship speed and state of various machinery present in the vessel [23,28], as well as ocean environmental propagation conditions, which can enhance measurement of the dominant tonal frequency components of sound radiated from a ship.

When the high source levels of the narrowband tonal or cyclostationary signal radiated from a ship are not appropriately accounted for, it can lead to incorrect estimates of the spatial extent of the ship-radiated sound field. For instance, if the POD region calculations for the 168.5 Hz and 808 Hz tonals radiated by the RV John Hjort and received on the coherent hydrophone array were based on the one-third octave bandwidth intensity averaged source level values at these frequencies, provided in Figure 2 of Ref. [23], the estimated POD regions would be extremely small (see cyan lines in Figure 11)) and could not explain the observed data.

The measurements of ship-radiated underwater sound have been applied to study the potential avoidance behavior of fish to ships and other underwater vehicles employed for fish echosounder and trawl sampling surveys [22–24,28–31]. It is believed that the 'vessel-induced fish behavior' may bias survey estimates of fish stock abundance. Previous studies have compared overall one-third octave bandwidth intensity averaged broadband ship-radiated sound source level for different ships or vehicles used for fish assessment surveys with the ICES-recommended one-third octave bandwidth-averaged source levels (CRR 209) for silent research vessels. These studies found no significant differences in response of fish to ships with contrasting one-third octave bandwidth averaged broadband ship-radiated source level that are above or below the ICES CRR 209 levels [22,30,31]. Here we find that the sound field radiated from an underwater vehicle is significantly dominated by their narrowband tonals with bandwidths that range from less than 1 Hz to about 3 Hz and source levels that may stand 10 dB to 30 dB above the one-third-octave bandwidth-averaged levels. Since the bandwidth of the dominant tonals are small (roughly 1 Hz), their levels get averaged out, and so is not accurately represented by one-third octave bandwidth averaging. The fish populations are more likely to sense the high level tonal signals than the lower level broadband sound. According to [22], the vessel stimulus to fish behavior investigated in that study were based on the one-third

octave bandwidth-averaged levels from RV Johan Hjort, and found to be an inappropriate parameter to quantify ship sound. Here we propose that the full unaveraged spectra should be used for investigation of fish behavior to properly account for the unusually high levels of tonal sounds from ships that the fish would be most sensitive to. Our findings are consistent with recommendations of Mitson in [23] regarding ship-radiated sound since the "smoothing effect of averaging can disguise very strong tones present in the true signature occurring within the hearing spectrum of fish".

In the fishery research community there has long been a focus on building noise-reduced research vessels according to recommendations provided by ICES [28]. Since then (1995) many research vessels have been built meeting these requirements. However, there is no reason to believe that these specially designed vessels do not suffer from some of the same extreme tonal sound levels as observed from conventionally designed vessels in our study. Therefore, some of these vessels should also be studied with our method to potentially explain the unexpected impacts from noise-reduced vessels like those described by Ref. [22].

5. Conclusions

The sound radiated underwater by three research and fisheries survey vessels have been detected and characterized from long ranges (4–32 km) with a large-aperture densely-sampled coherent hydrophone array using the passive ocean acoustic waveguide remote sensing (POAWRS) technique. The detected underwater sounds radiated from each of the three research and fishing vessels are found to be dominated by a number of narrowband tonals or cyclostationary signals in the 150 Hz to 2000 Hz frequency range. The temporal-spectral characteristics and source levels of the prominent tonals or cyclostationary signals have been quantified for each ship. The probability of detection regions for the most dominant signals of the RV Delaware II in the Gulf of Maine, and the RV Johan Hjort and the FV Artus in the Norwegian Sea are estimated and shown to extend over areas spanning roughly 200 km in diameter when employing a large-aperture densely-sampled coherent hydrophone array. The current standard procedure for quantifying ship-radiated sound source levels via one-third octave bandwidth intensity averaging smoothes over the prominent tonals radiated by a ship that can stand 10 dB to 30 dB above the local broadband level, which may lead to incorrect or inaccurate assessments of the impact of ship-radiated sound.

Appendix A. Modelling Probability of Detection Regions for Ship-Radiated Signals

The POAWRS probability of detection (POD) $P_D(r)$ for a ship-radiated signal as a function of range r from the coherent hydrophone array is modeled following the approach described in Section I of the Supplementary Information of [13] for POAWRS detection of marine mammal vocalization pulses, but is reformulated here for ship tonal and cyclostationary signal detection.

For a ship located at range r from the POAWRS receiver array, its radiated signal can be detected above the ambient noise if the sonar equation [9,33,76–78] is satisfied,

$$NL + DT - AG < L_S - TL(r), \tag{A1}$$

where L_S is the source level of the ship-radiated signal, NL is the ambient noise level in the frequency band of that signal, AG is the coherent beamforming gain of the passive receiver array, DT is the detection threshold, and TL is the broadband transmission loss.

The ship-radiated signals are detected from the beamformed spectrograms and typically occupy roughly M number of independent time-frequency pixels $\Delta f \Delta t$. We first calculate the detection probability $p_{D,1}(r)$ in a single frequency-time pixel using [9,79],

$$p_{D,1}(r) = \int_{-\infty}^{+\infty} f_{L_R}(L_R(r)) \int_{-\infty}^{L_R(r)-DT} f_{L_N}(L_N) dL_N dL_R, \tag{A2}$$

where $f_{L_N}(L_N)$ is the probability density function of the log-transformed ambient noise pressure-squared $L_N(t,f) = 10\log_{10}(|P_N(t,f)/P_{ref}|^2) = S_N(t,f) + 10\log_{10}(\Delta f) - AG$ within a single beamformed spectrogram time-frequency pixel in the frequency range of the ship-radiated signal, where $P_N(t,f)$ is the ambient noise pressure at time t within frequency bin Δf centered at frequency f and $S_N(t,f)$ is the omnidirectional ambient noise spectral density level; $f_{L_R}(L_R(r))$ is the probability density function of the received ship-radiated signal log-transformed pressure-squared $L_R(r|t,f) = 10\log_{10}(|P_R(r|t,f)/P_{ref}|^2) = L_S - TL(r) + 10\log_{10}\frac{\Delta f}{B(t)}$ within a single beamformed spectrogram time-frequency pixel, where $P_R(r|t,f)$ is the received ship-radiated signal pressure, and $B(t)$ is the instantaneous bandwidth of that signal at time t. The number of independent beamformed spectrogram frequency-time pixels occupied by the ship-radiated signal is related to the instantaneous bandwidth via $M\Delta f\Delta t = \tau B(t)$, where τ is the signal duration ($\tau \approx 20$ s). An exponential-Gamma distribution [1,57,80] describes the log-transformed ambient noise pressure-squared and log-transformed received ship-radiated signal pressure-squared within a single beamformed spectrogram time-frequency pixel,

$$f_{L_N}(L_N) = \frac{1}{(10\log_{10} e)\Gamma(\mu)}\left(\frac{\mu}{\langle P_N^2\rangle}\right)^{\mu} 10^{\mu L_N/10}\exp(-\mu\frac{10^{L_N/10}}{\langle P_N^2\rangle}) \tag{A3}$$

$$f_{L_R}(L_R(r)) = \frac{1}{(10\log_{10} e)\Gamma(\mu)}\left(\frac{\mu}{\langle P_R^2(r)\rangle}\right)^{\mu} 10^{\mu L_R(r)/10}\exp(-\mu\frac{10^{L_R(r)/10}}{\langle P_R^2(r)\rangle}), \tag{A4}$$

where μ is the time-bandwidth product or number of statistically independent fluctuations of the respective pressure-squared quantities. Since the beamformed spectrograms have time-frequency pixels that satisfy $\Delta f\Delta t = 1$, both the ambient noise level and the received ship-radiated signal level within each beamformed spectrogram time-frequency pixel can be treated as instantaneous with time-bandwidth product $\mu = 1$ and 5.6 dB standard deviation. For the received ship-radiated signal level, this standard deviation includes both the standard deviation of the ship-radiated signal source level, as well as the standard deviation of the broadband waveguide transmission loss. The 5.6-dB standard deviation used here for the received ship-radiated signal level is a good approximation to the standard deviations shown in Figures 6, 10 and 14.

We assume the received ship-radiated signal is detectable if it stands above the ambient noise in at least 30% of the M time-frequency pixels of the beamformed spectrogram. The overall probability of detection, $P_D(r)$, for the ship-radiated signal as a function of range r from the POAWRS receiver array is then calculated from the Gaussian approximation to the binomial cumulative distribution function (CDF) [79] as,

$$P_D(r) = 1 - \Phi(\frac{0.3M - Mp_{D,1}(r)}{\sqrt{Mp_{D,1}(r)(1-p_{D,1}(r))}}). \tag{A5}$$

where $\Phi(z) = \frac{1}{\sqrt{2\pi}}\int_{-\infty}^{z} e^{-u^2/2}du$. The Gaussian approximation to the binomial CDF is an appropriate model for the overall performance of the detector when considering the thousands of ship-radiated signals analyzed. The exponential-Gamma distribution [57,80] for the log-transform of Gaussian field measurements, used here to model the probability density function of the received ship-radiated signal level and the ambient noise level, has been calibrated with: (1) thousands of log-transformed intensity measurements from controlled source transmissions made during the same GOME06 discussed here at the same time and at the same location [57]; and (2) thousands of measurements made during a past experiment conducted in a similar continental shelf environment [54].

The omnidirectional ambient noise spectral density levels $S_N(f)$ are estimated directly from the POAWRS receiver array using data segments that are devoid of ship-radiated signals and other significant sound sources. The $S_N(f)$ (in units of dB re 1 $\mu Pa^2/Hz$) used are provided in Table A1.

Table A1. Estimates of ship-radiated narrowband tonal and cyclostationary signal source levels for the RV Delaware II, the RV Johan Hjort and the FV Artus.

Ships	Frequency (Hz)	Bandwidth (Hz)	Ship Signal Source Level (dB re 1 μPa/Hz at 1 m)	Unbeamformed Ambient Noise Level (dB re 1 μPa/Hz)
RV Delaware II	176.1	3.5 ± 1.7	148.7 ± 5.2	72.2
	573.0	0.8 ± 0.4	162.3 ± 6.0	67.0
RV Johan Hjort	168.5	0.8 ± 0.4	168.4 ± 7.2	86.0
	694.2	3.1 ± 1.4	147.6 ± 4.3	79.0
	808.3	1.9 ± 0.9	148.5 ± 4.0	77.4
FV Artus	170.3	1.3 ± 0.9	148.7 ± 2.1	81.7
	715.6	2.5 ± 1.4	143.5 ± 5.8	76.8
	1583.8	3.4 ± 2.1	133.5 ± 6.0	70.3
	1790.9	4.0 ± 1.7	130.0 ± 5.2	67.2

Acknowledgments: This research is supported by the Office of Naval Research (Ocean Acoustics Program), the National Science Foundation, the National Oceanographic Partnership Program, the U.S. Presidential Early Career Award for Scientists and Engineers, the Alfred P. Sloan Foundation, the Census of Marine Life, and Northeastern University.

Author Contributions: Data analysis and interpretation conducted primarily by Wei Huang, with contributions from Heriberto Garcia, Delin Wang and Purnima Ratilal; Wei Huang and Purnima Ratilal wrote the paper.

Conflicts of Interest: The authors declare no conflict of interest.

Abbreviations

The following abbreviations are used in this manuscript:

POAWRS	passive ocean acoustic waveguide remote sensing
OAWRS	ocean acoustic waveguide remote sensing
RV	research vessel
FV	fishing vessel
GPS	global positioning systems

References

1. Bergmann, P.G.; Yaspan, A.; Gerjuoy, E.; Major, J.K.; Wildt, R. (Eds.) *Physics of Sound in the Sea*; Gordon and Breach: Philadelphia, PA, USA, 1968.
2. Arveson, P.T.; Vendittis D.J. Radiated noise characteristics of a modern cargo ship. *J. Acoust. Soc. Am.* **2000**, *107*, 118–129.
3. Bruno, M.; Chung, K.W.; Salloum, H.; Sedunov, A.; Sedunov, N.; Sutin, A.; Mallas, P. Concurrent use of satellite imaging and passive acoustics for maritime domain awareness. In Proceedings of the 2010 International Waterside Security Conference (WSS), Carrara, Italy, 3–5 November 2010; pp. 1–8.
4. Chung, K.W.; Sutin, A.; Sedunov, A.; Bruno, M. DEMON acoustic ship signature measurements in an urban harbor. *Adv. Acoust. Vib.* **2011**, *2011*, 952798.
5. Fillinger, L.; Sutin, A.; Sedunov, A. Acoustic ship signature measurements by cross-correlation method. *J. Acoust. Soc. Am.* **2010**, *129*, 774–778.
6. Leal, N.; Leal, E.; Sanchez, G. Marine vessel recognition by acoustic signature. *ARPN J. Eng. Appl. Sci.* **2015**, *10*. Available online: http://www.arpnjournals.org/jeas/research_papers/rp_2015/jeas_1115_2919.pdf (accessed on 26 July 2017).
7. Ogden, G.L.; Zurk, L.M.; Jones, M.E.; Peterson, M.E. Extraction of small boat harmonic signatures from passive sonar. *J. Acoust. Soc. Am.* **2011**, *129*, 3768-3776.
8. Wales, S.C.; Heitmeyer, R.M. An ensemble source spectra model for merchant ship-radiated noise. *J. Acoust. Soc. Am.* **2002**, *111*, 1211–1231.
9. Urick, R.J. *Principles of Underwater Sound*, 3rd ed.; McGraw Hill: New York, NY, USA, 1983; pp. 29–65, 328–366.

10. Wenz, G.M. Acoustic Ambient Noise in the Ocean: Spectra and Sources. *J. Acoust. Soc. Am.* **1962**, *34*, 1936–1956.
11. Makris, N.C.; Ratilal, P.; Symonds, D.T.; Jagannathan, S.; Lee, S.; Nero, R.W. Fish population and behavior revealed by instantaneous continental shelf-scale imaging. *Science* **2006**, *311*, 660–663.
12. Makris, N.C.; Ratilal, P.; Jagannathan, S.; Gong, Z.; Andrews, M.; Bertsatos, I.; Godø, O.R.; Nero, R.W.; Jech, J.M. Critical Population Density Triggers Rapid Formation of Vast Oceanic Fish Shoals. *Science* **2009**, *323*, 1734–1737.
13. Wang, D.; Garcia, H.; Huang, W.; Tran, D.D.; Jain, A.D.; Yi, D.H.; Gong, Z.; Jech, J.M.; Godoe, O.R.; Makris, N.C.; et al. Vast assembly of vocal marine mammals from diverse species on fish spawning ground. *Nature* **2016**, *531*, 366–370.
14. MacLennan, D.N.; Simmonds, E.J. *Fisheries Acoustics*; Chapman and Hall: London, UK, 1992; Volume 5.
15. Stojanovic, M. Underwater acoustic communications. In Proceedings of the Professional Program Electro/95 International, Boston, MA, USA, 21–23 June 1995; pp. 435–440.
16. Stojanovic, M.; Preisig, J. Underwater acoustic communication channels: Propagation models and statistical characterization. *IEEE Commun. Mag.* **2009**, *47*, 84–89.
17. Dambra, R.; Firenze, E. Underwater Radiated Noise of a Small Vessel. In Proceedings of the 22nd International Congress on Sound and Vibration, Orence, Italy, 12–16 July 2015.
18. Hildebrand, J.A. Anthropogenic and natural sources of ambient noise in the ocean. *Mar. Ecol. Prog. Ser.* **2009**, *395*, 5–20.
19. Merchant, N.D.; Witt, M.J.; Blondel, P.; Godley, B.J.; Smith, G.H. Assessing sound exposure from shipping in coastal waters using a single hydrophone and Automatic Identification System (AIS) data. *Mar. Pollut. Bull.* **2012**, *64*, 1320–1329.
20. Vasconcelos, R.O.; Amorim, M.C.P.; Ladich, F. Effects of ship noise on the detectability of communication signals in the Lusitanian toadfish. *J. Exp. Biol.* **2007**, *210*, 2104–2112.
21. Codarin, A.; Wysocki, L.E.; Ladich, F.; Picciulin, M. Effects of ambient and boat noise on hearing and communication in three fish species living in a marine protected area (Miramare, Italy). *Mar. Pollut. Bull.* **2009**, *58*, 1880–1887.
22. Ona, E.; Godø, O.R.; Handegard, N.O.; Hjellvik, V.; Patel, R.; Pedersen, G. Silent research vessels are not quiet. *J. Acoust. Soc. Am.* **2007**,*121*, EL145–EL150.
23. Mitson, R.B. Underwater noise radiated by research vessels. *ICES Mar. Sci. Symp.* **1993**, *196*, 147–152.
24. Mitson, R.B.; Knudsen, H.P. Causes and effects of underwater noise on fish abundance estimation. *Aquat. Living Resour.* **2003**, *16*, 255–263.
25. Hatch, L.; Clark, C.; Merrick, R.; Van Parijs, S.; Ponirakis, D.; Schwehr, K.; Thompson, M.; Wiley, D. Characterizing the relative contributions of large vessels to total ocean noise fields: A case study using the Gerry E. Studds Stellwagen Bank National Marine Sanctuary. *Environ. Manag.* **2008**, *42*, 735–752.
26. Veirs, S.; Veirs, V.; Wood, J.D. Ship noise extends to frequencies used for echolocation by endangered killer whales. *PeerJ* **2016**, *4*, e1657.
27. Wittekind, D.K. A simple model for the underwater noise source level of ships. *J. Ship Rrod. Design* **2014**, *30*, 7–14.
28. Mitson, R.B. *Underwater Noise of Research Vessels*; ICES Co-Operative Research Report; ICES: Copenhagen, Denmark, 1995; Volume 61.
29. Fernandes, P.G.; Brierley, A.S.; Simmonds, E.J.; Millard, N.W.; McPhail, S.D.; Armstrong, F.; Stevenson, P.; Squires, M. Oceanography: Fish do not avoid survey vessels. *Nature* **2000**, *404*, 35–36.
30. Jørgensen, R.; Handegard, N.O.; Gjøsæter, H.; Slotte, A. Possible vessel avoidance behaviour of capelin in a feeding area and on a spawning ground. *Fish. Res.* **2004**, *69*, 251–261.
31. De Robertis, A.; Handegard, N.O. Fish avoidance of research vessels and the efficacy of noise-reduced vessels: A review. *ICES J. Mar. Sci.* **2013**, *70*, 34–45.
32. Huang, W.; Wang, D.; Ratilal, P. Diel and Spatial Dependence of Humpback Song and Non-Song Vocalizations in Fish Spawning Ground. *Remote Sens.* **2016**, *8*, 712.
33. Gong, Z.; Jain, A.D; Tran, D.D.; Yi, D.H.; Wu, F.; Zorn, A.; Ratilal, P.; Makris, N.C. Ecosystem scale acoustic sensing reveals humpback whale behavior synchronous with herring spawning processes and re-evaluation finds no effect of sonar on humpback song occurrence in the Gulf of Maine in Fall 2006. *PLoS ONE* **2014**, *9*, e104733.

34. Tran, D.D; Huang, W.; Bohn, A.C; Wang, D.; Gong, Z.; Makris, N.C; Ratilal, P. Using a coherent hydrophone array for observing sperm whale range, classification, and shallow-water dive profiles. *J. Acoust. Soc. Am.* **2014**, *135*, 3352–3363.
35. Wang, D.; Huang, W.; Garcia, H.; Ratilal, P. Vocalization source level distributions and pulse compression gains of diverse baleen whale species in the Gulf of Maine. *Remote Sens.* **2016**, *8*, 881.
36. Crocker, S.E.; Nielsen, P.L.; Miller, J.H.; Siderius, M. Geoacoustic inversion of ship radiated noise in shallow water using data from a single hydrophone. *J. Acoust. Soc. Am.* **2014**, *136*, EL362–EL368.
37. Hallett, M.A. Characteristics of merchant ship acoustic signatures during port entry/exit. In Proceedings of the Acoustics, Gold Coast, Australia, 3–5 November 2004; pp. 3–5.
38. Sutin, A.; Bunin, B.; Sedunov, A.; Sedunov, N.; Fillinger, L.; Tsionskiy, M.; Bruno, M. Stevens passive acoustic system for underwater surveillance. In Proceedings of the 2010 International Waterside Security Conference (WSS), Carrara, Italy, 3–5 November 2010; pp. 1–6.
39. Nejedl, V.; Stoltenberg, A.; Schulz, J. Free-field measurements of the radiated and structure borne sound of RV Planet. *Proc. Meet. Acoust.* **2012**, *17*, 070061. doi:10.1121/1.4773107.
40. McKenna, M.F.; Ross, D.; Wiggins, S.M.; Hildebrand, J.A. Underwater radiated noise from modern commercial ships. *J. Acoust. Soc. Am.* **2012**, *131*, 92–103.
41. Fréchou, D.; Dugué, C.; Briançon-Marjollet, L.; Fournier, P.; Darquier, M.; Descotte, L.; Merle, L. Marine Propulsor Noise Investigations in the Hydroacoustic Water Tunnel "GTH". In Proceedings of the Twenty-Third Symposium on Naval Hydrodynamics, Val de Reuil , France, 17–22 September 2000.
42. Bush V.; Conant J.B.; Tate J.T. *Principles and Applications of Underwater Sound*; Summary Technical Report; Office of Scientific Research and Development: Washington DC, USA, 1946; Volume 7.
43. Norwood, C. An introduction to ship radiated noise. *Acoust. Aust.* **2002**, *30*, 21–25.
44. Ojak, W. Vibrations and waterborne noise on fishery vessels. *J. Ship Res.* **1988**, *32*, 112–133.
45. Gray, L.M.; Greeley, D.S. Source level model for propeller blade rate radiation for the world's merchant fleet. *J. Acoust. Soc. Am.* **1980**, *67*, 516–522.
46. Grelowska, G.; Kozaczka, E.; Kozaczka, S.; Szymczak, W. Underwater noise generated by a small ship in the shallow sea. *Arch. Acoust.* **2013**, *38*, 351–356.
47. Malinowski, S.J.; Gloza, I. Underwater noise characteristics of small ships. *Acta Acust. United Acust.* **2002**, *88*, 718–721.
48. Gloza, I. Identification methods of underwater noise sources generated by small ships. *Acta Phys. Pol. A* **2011**, *119*, 961–965.
49. Gloza, I.; Malinowski, S. Identification of ships underwater noise sources in the coastal region. *Hydroacoustics* **2003**, *5*, 9–16.
50. Sandhya, M.; Rajarajeswari, K.; Seetaramaiah, P. Detecting Inception of Hydrodynamic cavitation Noise of Ships using Quadratic Phase coupling Index as an Indicator. *Def. Sci. J.* **2015**, *65*, 53–62.
51. Trevorrow, M.V.; Vasiliev, B.; Vagle, S. Directionality and maneuvering effects on a surface ship underwater acoustic signature. *J. Acoust. Soc. Am.* **2008**, *124*, 767–778.
52. Ianniello, S.; Muscari, R.; Di Mascio, A. Ship underwater noise assessment by the acoustic analogy. Part I: Nonlinear analysis of a marine propeller in a uniform flow. *J. Mar. Sci. Technol.* **2013**, *18*, 547–570.
53. Shioiri, An Aspect of the Propeller-Singing Phenomenon as a Self-Excited Oscillation; Davidson Laboratory Report 1059. Available online: http://www.dtic.mil/get-tr-doc/pdf?AD=AD0464615 (accessed on 26 July 2017).
54. Andrews, M.; Chen, T.; Ratilal, P. Empirical dependence of acoustic transmission scintillation statistics on bandwidth, frequency and range in New Jersey continental shelf. *J. Acoust. Soc. Am.* **2009**, **125**, 111–124.
55. Andrews, M.; Gong, Z.; Ratilal, P. Effects of multiple scattering, attenuation and dispersion in waveguide sensing of fish. *J. Acoust. Soc. Am.* **2011**, *130*, 1253–1272.
56. Gong, Z.; Andrews, M.; Jagannathan, S.; Patel, R.; Jech, J.M.; Makris, N.C.; Ratilal, P. Low-frequency target strength and abundance of shoaling Atlantic herring (*Clupea harengus*) in the Gulf of Maine during the Ocean Acoustic Waveguide Remote Sensing 2006 Experiment. *J. Acoust. Soc. Am.* **2010**, *127*, 104–123.
57. Tran, D.; Andrews, M.; Ratilal, P. Probability distribution for energy of saturated broadband ocean acoustic transmission: Results from Gulf of Maine 2006 experiment. *J. Acoust. Soc. Am.* **2012**, *132*, 3659–3672.
58. Collins, M.D. A split step Padé solution for the parabolic equation method. *J. Acoust. Soc. Am.* **1993**, *93*, 1736–1742.

59. Collins, M.D.; Westwood, E. K. A higher-order energy-conserving parabolic equqation for range-dependent ocean depth, sound speed, and density. *J. Acoust. Soc. Am.* **1991**, *89*, 1068–1075.
60. Gong, Z.; Tran, D.D.; Ratilal, P. Comparing passive source localization and tracking approaches with a towed horizontal receiver array in an ocean waveguide. *J. Acoust. Soc. Am.* **2013**, *134*, 3705–3720.
61. Jagannathan, S.; Kusel, E.T.; Ratilal, P.; Makris, N.C. Scattering from extended targets in range-dependent fluctuating ocean-waveguides with clutter from theory and experiments. *J. Acoust. Soc. Am.* **2012**, *132*, 680–693.
62. Jagannathan, S.; Bertsatos, I.; Symonds, D.; Chen, T.; Nia, H.T.; Jain, A.D.; Jech, M. Ocean acoustic waveguide remote sensing (OAWRS) of marine ecosystems. *MEPS* **2009**, *395*, 137–160.
63. Overholtz, W.J.; Jech, J.M.; Michaels, W. L.; Jacobson, L.D.; Sullivan, P.J. Empirical comparisons of survey designs in acoustic surveys of Gulf of Maine-Georges Bank Atlantic herring. *J. Northw. Atl. Fish. Sci.* **2006**, *36*, 127–144.
64. Weinberg, J. *54th Northeast Regional Stock Assessment Workshop (54th SAW) Assessment Report*; Northeast Fisheries Science Center Reference Document 12-18; Northeast Fisheries Science Center: Woods Hole, MA, USA, 2012.
65. Jech, J.M.; Stroman, F. Aggregative patterns of pre-spawning Atlantic herring on Georges Bank from 1999–2010. *Aquat. Living Resour.* **2012**, *25*, 1–14.
66. Becker, K.; Preston, J.R. The ONR Five Octave Research Array (FORA) at Penn State. *IEEE J. Ocean Eng.* **2003**, *5*, 2607–2610.
67. Ratilal, P.; Lai, Y.S.; Symonds, D.T.; Ruhlmann, L.A.; Preston, J.R.; Scheer, E.K.; Garr, M.T.; Holland, C.W.; Goff, J.A.; Makris, N.C. Long range acoustic imaging of the continental shelf environment: The Acoustic Clutter Reconnaissance Experiment 2001. *J. Acoust. Soc. Am.* **2005**, *1117*, 1977–1998.
68. Jain, A.D. Instantaneous Continental-Shelf Scale Sensing of Cod with Ocean Acoustic Waveguide Remote Sensing (OAWRS). Ph.D. Thesis, Massachusetts Institute of Technology, Cambridge, MA, USA, 2015.
69. Kay, S.M. *Fundamentals of Statistical Signal Processing, Volume II: Detection Theory*; Prentice-Hall: Upper Saddle River, NJ, USA, 1993; pp. 375–380.
70. Johnson, D.H.; Dudgeon, D.E. *Array Signal Processing: Concepts and Techniques*; Simon & Schuster: New York, NY, USA, 1992; pp. 1–512.
71. Baumgartner, M.F.; Mussoline, S.E. A generalized baleen whale call detection and classification system. *J. Acoust. Soc. Am.* **2011**, *129*, 2889–2902.
72. Shapiro, A.D.; Wang, C. A versatile pitch tracking algorithm: From human speech to killer whale vocalizations. *J. Acoust. Soc. Am.* **2009**, *126*, 451–459.
73. Kinsler, L.E.; Frey, A.R.; Coppens, A.B.; Sanders, J.V. *Fundamentals of Acoustics*, 4th ed.; Wiley-VCH: New York, NY, USA, 1999; p. 448.
74. Da Costa, E.L. *Detection and Identification of Cyclostationary Signals*; Naval Postgraduate School: Monterey, CA, USA, 2007.
75. Blake, W. K. Periodic and random excitation of streamlined structures by trailing edge flows. In *Turbulence in Liquids*; Science Press: Princeton, NJ, USA, 1977; pp. 167–178.
76. Burdic, W.S. *Underwater Acoustic System Analysis*; Prentice Hall: Upper Saddle River, NJ, USA, 1991; pp. 322–360.
77. Clay, C. S.; Medwin, H. *Acoustical Oceanography: Principles and Applications*; John Wiley & Sons: New York, NY, USA, 1977; pp. 494–501.
78. Jensen, F.B.; Kuperman, W.A.; Porter, M.B.; Schmidt, H. *Computational Ocean Acoustics* 2nd ed.; Springer Science & Business Media: Berlin, Germany, 2011; pp. 708–713.
79. DiFranco, J.V.; Rubin, W.L. *Radar Detection*; Artech House Inc.: Dedham, MA, USA, 1980.
80. Makris, N.C. The effect of saturated transmission scintillation on ocean acoustic intensity measurements. *J. Acoust. Soc. Am.* **1996**, *100*, 769–783.